DEFENCE R&D DÉFENSE

Performance of RADARSAT2 SAR-GMTI Processors at High SAR Resolutions

Shen Chiu
Defence Research Establishment Ottawa

Defence R&D Canada

DEFENCE RESEARCH ESTABLISHMENT OTTAWA

TECHNICAL REPORT
DREO TR 2000-093
November 2000

National Defence Défense nationale

Canada

DEFENCE R&D DÉFENSE

Performance of RADARSAT2 SAR-GMTI Processors at High SAR Resolutions

Shen Chiu
Space Systems Group
Space Systems and Technology Section

DEFENCE RESEARCH ESTABLISHMENT OTTAWA

TECHNICAL REPORT
DREO TR 2000-093
November 2000

Project
5EG11

Abstract

Canada's RADARSAT2 commercial Synthetic Aperture Radar (SAR) satellite, scheduled to be launched in Spring 2003, will have an experimental operating mode that will permit Ground Moving Target Indication (GMTI) measurements to be made with received data. In this mode of operation, the radar antenna is partitioned into two sub-apertures that sequentially observe the scene of interest from the same points in space. Two GMTI processing approaches are currently being explored. One utilizes the classical SAR/DPCA (Displaced Phase Center Antenna) clutter cancellation technique to provide sub-clutter visibility for dim slowly moving objects. The other is based on the Along-Track Interferometric SAR (SAR/ATI) technique, where amplitude and phase information of the targets are exploited to extract them from the background clutter. In this paper the performance of each processor is examined for RADARSAT2's ultrafine beam mode. The study focuses on the influence of SAR resolution cell size on the GMTI processor performance. Results indicate that at high SAR resolutions the SAR/ATI is a better technique compared to the SAR/DPCA in its ability to detect slow-moving targets.

Résumé

Le satellite RAS commercial RASARSAT2 du Canada, dont le lancement est prévu pour le printemps 2003, sera pourvu d'un mode de fonctionnement expérimental qui permettra de mesurer les indications de cibles terrestres mobiles (GMTI) à partir des données reçues. Dans ce mode, l'antenne du radar se divise en deux ouvertures qui observent la scène d'intérêt successivement à partir des mêmes points de l'espace. On étudie actuellement deux méthodes de traitement GMTI. La première est basée sur la technique classique d'élimination de fouillis RAS/DPCA, qui produit une visibilité sous fouillis des cibles à mouvements lents et indistincts. La deuxième repose sur la technique de l'interféromètre longitudinal (temporel) RAS (RAS/ATI), où les informations sur l'amplitude et la phase des cibles sont exploitées afin de les extraire du fouillis fixe. Dans cet article, la performance de chaque processeur est examinée pour les modes faisceau fin de RADARSAT2. L'examen porte particulièrement sur l'influence de la grandeur des cellules de résolution RAS sur la performance du processeur GMTI. Les résultats indiquent qu'à de hautes résolutions, la technique RAS/ATI est meilleure par rapport à la technique RAS/DPCA quant à la capacité de détecter des cibles à mouvements lents.

Executive summary

Two Ground Moving Target Indication (GMTI) processing approaches are currently being developed for Canada's RADARSAT2 Moving Object Detection Experiment (MODEX) mode. One utilizes the classical Synthetic Aperture Radar, Displaced Phase Center Antenna (SAR/DPCA) clutter cancellation technique to provide sub-clutter visibility for dim slowly moving objects. The other is based on the Along-Track Interferometric SAR (SAR/ATI) technique, where amplitude and phase information of the targets are exploited to extract them from the clutter background. In this study the performance of each processor is examined for RADARSAT2 fine beam modes. The study focuses on the influence of SAR resolution on the processor performance.

Results indicate that, at high SAR resolutions, the SAR/ATI processor performs better than the SAR/DPCA processor in detecting slow-moving targets. Possible reasons for the observed difference in the processors' performance include an enhanced noise background due to a larger noise bandwidth and a reduced clutter contribution to the target signal due to a smaller resolution cell size at the high resolution mode. Being a noise-limited detector, the SAR/DPCA performance is directly affected by the increase in the noise background. The SAR/ATI detector, on the other hand, is a clutter-limited detector. It is, therefore, not very sensitive to the increase in noise because it does not rely on clutter suppression to extract targets and also because the target signal is squared in the SAR/ATI processing, thus, improving its signal-to-noise ratio.

The processors' performance is also examined for high-speed targets (> 100 km/h). Unlike the low speed case, the two GMTI processors do not show noticeable differences in their ability to detect high-speed targets. The result suggests that the velocity mismatch between the matched filter and the targets may have significantly reduced the targets' signal to the extent that the SAR/ATI detector may have also become noise-limited as the SAR/DPCA. The effect of the filter mismatch on the targets' signal amplitude is clearly demonstrated in a set of experiments using velocity-offset matched filters.

Chiu, S. 2000. Performance of RADARSAT2 SAR-GMTI Processors at High SAR Resolutions. DREO TR 2000-093. Defence Research Establishment Ottawa.

Sommaire

On conçoit actuellement deux approches de traitement GMTI pour le mode MODEX (expérience de détection d'objets mobiles) de RADARSAT2. La première est basée sur la technique classique d'élimination de fouillis RAS/DPCA, qui produit une visibilité sous fouillis des cibles à mouvements lents et indistincts. La deuxième repose sur la technique de l'interféromètre longitudinal (temporel) RAS (RAS/ATI), où les informations sur l'amplitude et la phase des cibles sont exploitées afin de les extraire du fouillis fixe. Dans cette étude, on examine la performance de chaque processeur pendant les modes faisceau fin de RADARSAT2. L'examen vise particulièrement l'influence de la résolution RAS sur la performance des processeurs.

Les résultats indiquent qu'à hautes résolutions, la performance du RAS/ATI est supérieure à celle du RAS/DPCA quant à détecter des cibles à mouvements lents. On pourrait entre autres attribuer la différence observée à un bruit de fond accentué par une bande de bruit plus large en modes haute résolution. L'augmentation de bruit de fond influe directement sur la performance du RAS/DPCA étant donné que celui-ci est détecteur à bruit réduit. Par contraste, le détecteur ATI n'est pas sensible à l'augmentation de bruit, parce qu'il ne fait pas appel à la suppression de fouillis pour dégager les cibles et, de plus, parce que le signal de cible est élevé au carré dans le traitement RAS/ATI, améliorant ainsi le rapport signal-bruit.

On a aussi étudié la performance des processeurs pour les cibles à haute vitesse (> 100 km/h). Contrairement au cas des cibles à mouvements lents, on n'a pas noté de différences perceptibles entre les deux processeurs GMTI quant à leur capacité de détecter des cibles à haute vitesse. Le résultat implique que l'écart de vitesse entre le filtre adapté et les cibles ont pu réduire les signaux des cibles considérablement à tel point que le détecteur RAS/ATI a pu aussi devenir un détecteur à bruit réduit comme le RAS/DPCA.

Chiu, S. 2000. Performance of RADARSAT2 SAR-GMTI Processors at High SAR Resolutions. DREO TR 2000-093. Le Centre de recherches pour la défense Ottawa.

Table of contents

List of figures

List of tables

Acknowledgements

Special thanks to Dr. Chuck Livingstone for his valuable advice and guidance throughout this work and to Georgio DiNardo for his computer support. This work is supported by the DREO Space Systems Group.

1. Introduction

Up to the present time, the detection and tracking of moving targets has been a primarily military concern and has been operationally supported by specialized airborne sensors. With the rapid evolution of radar technology it is now feasible to economically create spaceborne sensors to perform moving target detection and measurement functions. From a military viewpoint, these spaceborne systems have the potential to significantly augment existing operational capabilities. From a civilian viewpoint, spaceborne moving target measurements can provide a previously unavailable land and sea traffic monitoring capability that may prove to be very valuable in designing, monitoring, and controlling transportation infrastructure. Canada's RADARSAT2 (R2) commercial SAR satellite, scheduled to be launched in Spring 2003, will have an experimental operating mode that will allow ground moving target indication (GMTI) measurements to be made with received data. This mode is also called MODEX for Moving Object Detection Experiment. In the MODEX mode of operation, the spacecraft's radar antenna is partitioned into two apertures that sequentially observe the scene of interest from the same points in space. Data is simultaneously and coherently received from both apertures and is down-linked in parallel channels for processing to extract moving target radial speeds in their SAR image context. This paper provides an analysis of SAR-GMTI performance based on computer modeling and simulations. Two SAR-GMTI processing approaches are being explored. One utilizes the classical SAR/DPCA clutter cancellation technique to provide sub-clutter visibility for dim slowly moving targets. The other is based on the along-track (temporal) SAR interferometer (SAR/ATI) technique, where amplitude and phase information of the slow-moving targets are exploited to extract them from the dominant clutter background. The performance of each approach is examined for R2's ultrafine beam mode. The ultrafine mode is simply the highest resolution or bandwidth (100 MHz) supported by R2.

The present investigation focuses on the influence of the SAR resolution cell size on the two processors' performance. Due to SAR's finite resolution, clutter signals within the cell containing a moving target are added to the target's signal vectorially. The moving target's SAR/ATI signal phase is therefore reduced by the clutter signal vector, which lies along the zero-phase line in the complex plane. The effect of clutter contamination may be minimized if the target's physical size is comparable to the area of the resolution cell or if the overall clutter contribution is small compared to the target signal, in which case the performance of the SAR/ATI processor is expected to improve. The goal of this study is, therefore, to examine the effect of the SAR resolution on the R2 GMTI performance.

2.0 GMTI Processor Architectures

The proposed GMTI processor architectures for RADARSAT2 MODEX are shown in Figure 2.1. The SAR/DPCA processor (see Figure 2.1a) is the limiting case of the two-beam DPCA clutter canceller. The pulses from the leading antenna are delayed by T, the integral pulse number needed to effectuate the DPCA condition. SAR processing is then performed on each channel. The outputs of the SAR modules are subsequently subtracted to yield a GMTI image. The stationary clutter signals are suppressed, and only signals from moving targets with sufficient radial velocity remain. The use of the SAR/DPCA technique to provide SAR and MTI simultaneously has been discussed by other authors [1, 2]. Similarly, the SAR/ATI processor uses two-displaced phase centers aligned along-track, but instead of taking the difference of the two channels, the interferometric phase is computed. This is done by computing the phase or the complex argument of the product of one image with the complex conjugate of the other (see Figure 2.1b). The remaining phase is zero for stationary objects and non-zero otherwise. The application of the SAR/ATI technique to GMTI has also been discussed by other investigators [3, 4].

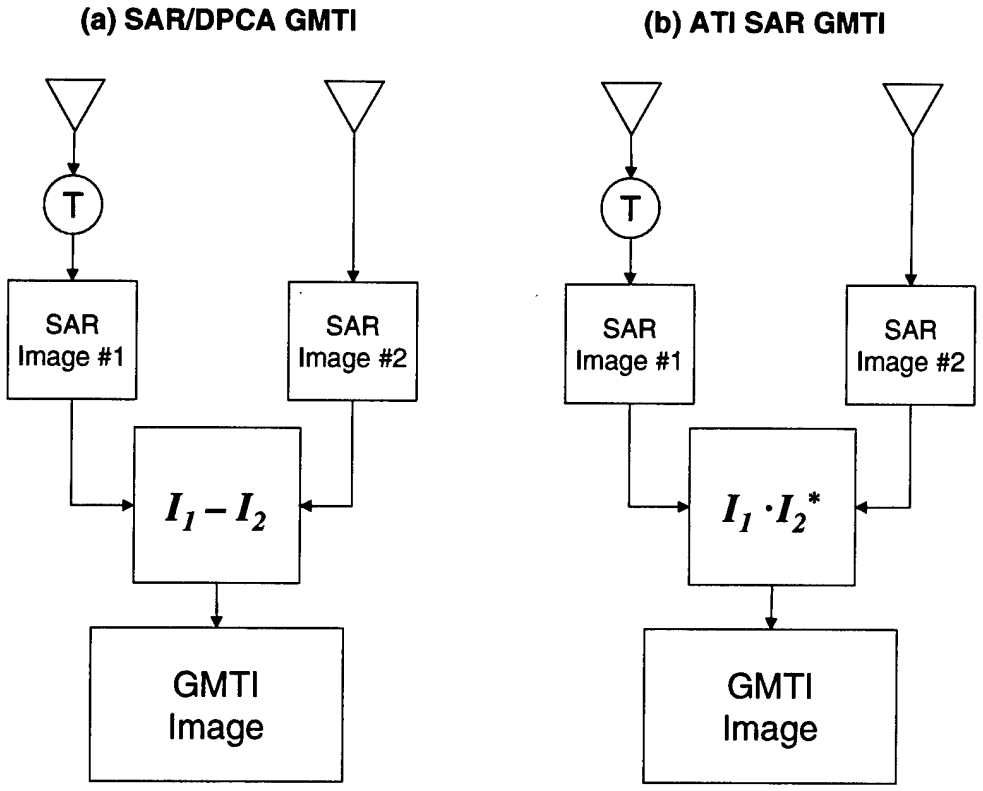

Figure 2.1 *Two simple SAR-GMTI processor architectures: (a) SAR/DPCA GMTI and (b) SAR/ATI GMTI.*

3.0 RADARSAT2 GMTI Mode

The RADARSAT2 MODEX is the world's first attempt to implement a limited-function GMTI aboard a commercial SAR satellite. Although the subset of possible GMTI operating modes available from a radar of this type is small, such a radar could be used to validate GMTI parameters and algorithms needed for more sophisticated radars. Preliminary information on the RADARSAT2 MODEX configuration can be found in references [5, 6]. Table 3.1 lists some of the SAR-MTI sensor characteristics and design parameters.

Table 3.1 *RADARSAT2 MODEX Parameters*

Parameter	Value
Orbit Description:	
Type	Circular
Inclination	98.6°
Altitude	800 km
Active Array:	
Length × Width	15 m × 1.5 m
Number of sub-apertures	2
Orientation	Long-axis forward, Elevation boresight ±29.5° (selectable)
Look Geometry:	
Nominal Incidence Angle	10° to 60°
Search Type	Strip-map
Swath Size	150 km to 25 km
Azimuth Beam Width	Programmable from 0.21° to 0.63°
Detection Cell Size	Programmable from 25m×25m to 3m×3m
Waveform:	
Band	5.405 GHz
Bandwidth	10 to 100 MHz
Peak Radiated Power	2.4 kW (42 μs pulse) 3.7 kW (21 μs pulse)
Duty Ratio	10 %
PRF	1300 to 3800 Hz
Burst Length	up to 500 ms
Receiver Noise Temperature:	695 K

4.0 SBRMTISIM Simulator

The simulation results described in the next section are obtained using a sophisticated space-based MTI radar simulator known as the SBRMTISIM, developed by Sicom Systems Ltd. for DND. The simulator provides an Environment Definition Window showing a world map overlaid with the satellite ground track (see Figure 4.1). The user can specify the look-geometry and define clutter regions and targets to create a scenario. Clutter is modeled as a set of regularly distributed scatterers with user specified cross-section, statistics and internal motion. Targets are modeled as point scatterers with user specified cross-section and fading statistics. Other windows are used to specify the radar and antenna parameters, and other parameters needed to characterize the system. Once these parameters are specified, the simulator generates high-fidelity, complex baseband signals representing the signals received by the SBR. The complete, two-way path of the signal is modeled from the transmitter, to the earth, and back to the receivers.

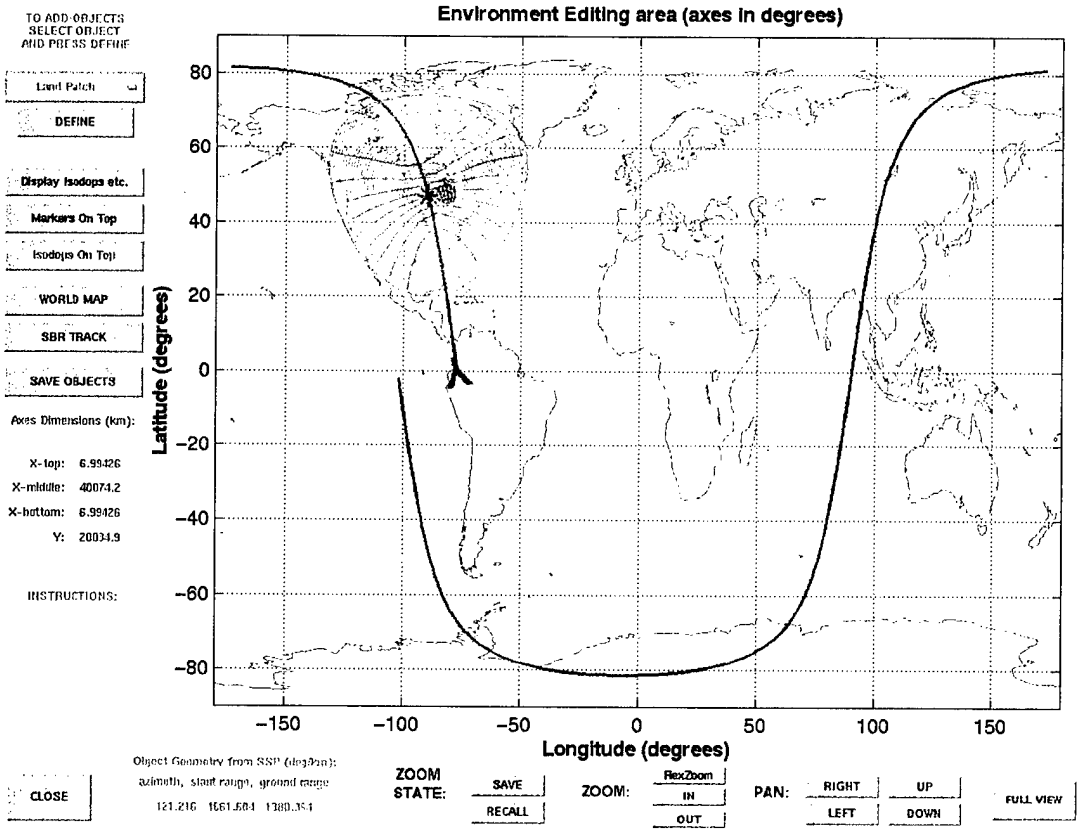

Figure 4.1 *SBRMTISIM Environment Definition Window*

5. Experiments

5.1 Experiment #1: Low Speeds

5.1.1. Experimental Definition

The first simulation experiment is carried out in the R2 ultrafine mode. The ultrafine beam is not supported by the R2 MODEX mode, but for the purpose of examining the effect of the resolution cell size on the processor performance, simulations are carried out in this mode of operation. The radar parameters used in the simulation, which we will call Scenario 1, are summarized in Table 5.1.1. The detailed radar and target parameters are listed in Appendix A.

Table 5.1.1 *Radar System Parameters: Scenario 1*

Peak power	5120 W	Noise temperature	1893 K
Carrier frequency	5.4 GHz	PRF	1988.3 Hz
Pulse width	21 μs	A/D sampling rate	112.6 M Hz
Pulse Bandwidth	100 MHz	Waveform	LFM
Burst length	0.75 s	Model receiver	Yes
IF bandwidth	112 MHz	IF center frequency	1500 MHz
IF filter type	Butterworth	IF filter order	8
Chan-to-chan mismatch.	-50 dB	A/D quantization level	-100
Number of A/D bits	8	No. of mismatch ripples	4
Radar system loss	0 dB		

The land patch used in this simulation run is the same as the one used in the R2 standard mode described in the paper submitted to NATO RTO (SET) conference, Samos, Greece [7]. However, the spacing between scatterers is changed from 10 m longitude and 4 m latitude to 2 m longitude and 4 m latitude. This is to ensure a minimum of one or two scatterers per resolution cell.

Also, in order to reduce the signal generation time to a reasonable time length, it is necessary to increase the "Available Memory" value in the "Signal Generation Seeds" Window from 200 MB to 800 MB. Due to the huge amount of data generated in the ultrafine mode, the SBRMTISIM software partitions the scatterers into a number of iteration blocks for radar signal generation according to specified memory availability for the hardware in use. The computation time increases rapidly with an increasing number of blocks.

The generated signals are passed through the SAR/ATI and SAR/DPCA processors. The results are presented below.

5.1.2 Results

The targets used in generating the ultrafine mode signals are the same as those used in the standard mode [7]. They are positioned in the clutter region as shown in Figure 5.1.1 and some of their properties are summarized in Table 5.1.2.

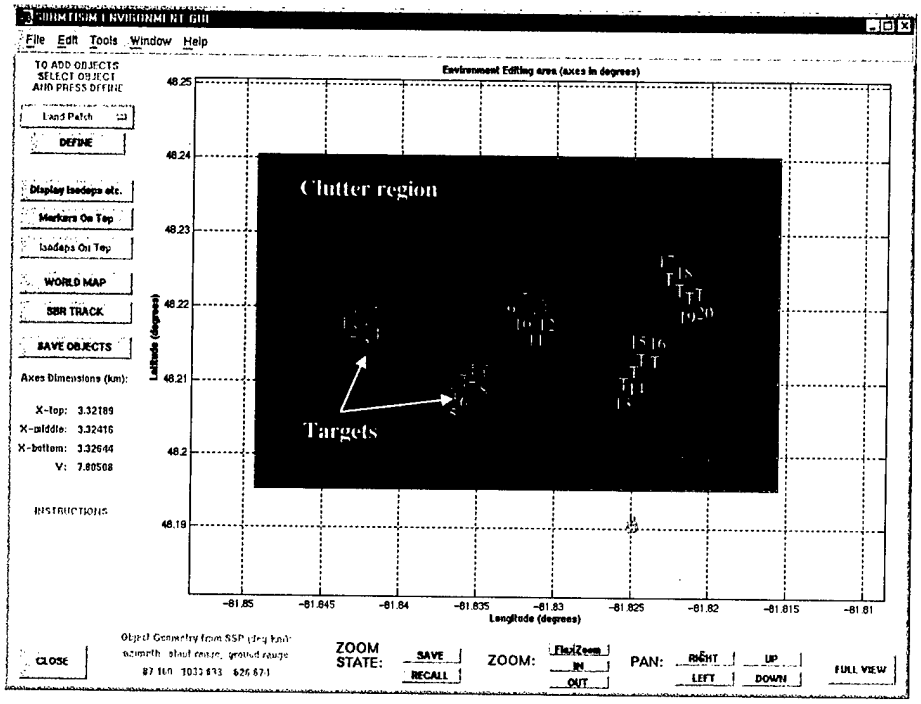

Figure 5.1.1 *SBRMTISIM environment window showing the 20 moving targets: Scenario 1*

Twenty targets occupy the clutter region and cover a typical range of radial speeds and target radar cross-sections (RCSs). As in the standard mode [7], the satellite heading is approximately north with right-looking geometry and the targets are heading either east or west. The only difference between the two modes is the higher bandwidth waveform used here. Specifically, the following changes from the standard mode to the ultrafine mode should be noted:

- Pulse bandwidth = 100 MHz instead of 11.58 MHz
- Sampling rate = 112.6 MHz instead of 12.66 MHz
- IF bandwidth = 112 MHz instead of 12 MHz

Table 5.1.2 *Target Parameters: Scenario 1*

Target Number	RCS (m^2)	Speed (m/s)
1	45	15 (east)
2	45	10 (east)
3	45	5 (east)
4	45	3 (east)
5	40	15 (west)
6	40	10 (west)
7	40	5 (west)
8	40	3 (west)
9	35	15 (east)
10	35	10 (east)
11	35	5 (east)
12	35	3 (east)
13	30	15 (west)
14	30	10 (west)
15	30	5 (west)
16	30	3 (west)
17	20	15 (east)
18	20	10 (east)
19	20	5 (east)
20	20	3 (east)

Plotting a 3D histogram of the SAR/ATI processor output, which is a complex signal matrix, in terms of its amplitude and phase, one gets a fin-like distribution as shown in Figure 5.1.2. Applying a moving target detection scheme similar to the one described in Reference [7], one obtains a detector of the form:

$$x < 20|y|^{3.3} - 0.12$$

Where x and y are in-phase and quadrature components, respectively, of the SAR/ATI output complex signal. This detector filters out the clutter signal and allows only the moving targets, with amplitude and phase values falling inside the detection region, to go through and be detected as shown in Figure 5.1.3. The output of this detector is plotted in Figure 5.1.4. The detector has a probability of false alarm, P_{FA}, of ~5×10^{-6}.

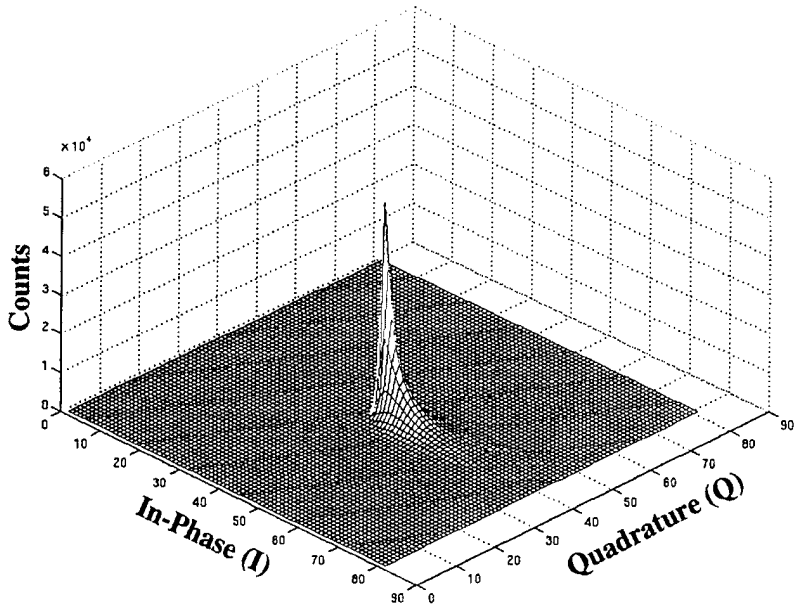

Figure 5.1.2 *3D histogram of the SAR/ATI processor complex signal output.*

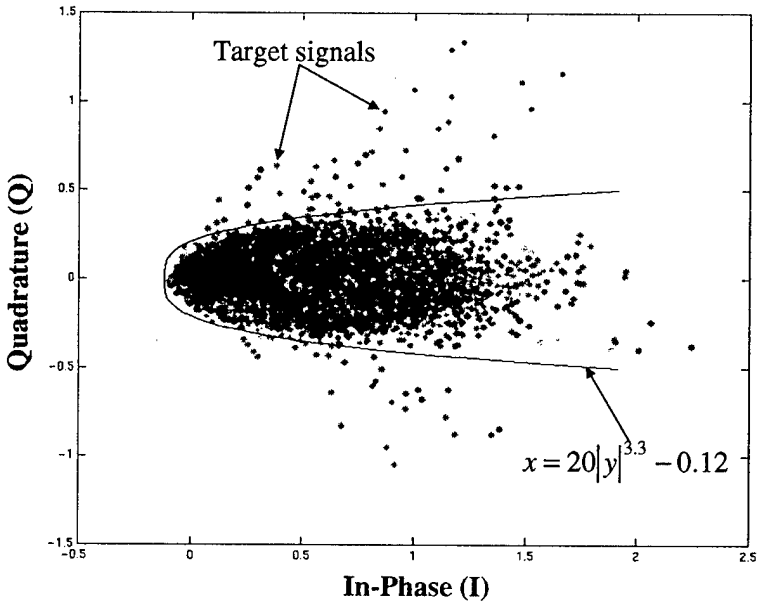

Figure 5.1.3 *The "$x = 20|y|^{3.3} - 0.12$" detector filters out the clutter signal and allows the moving targets signals to go through and be detected.*

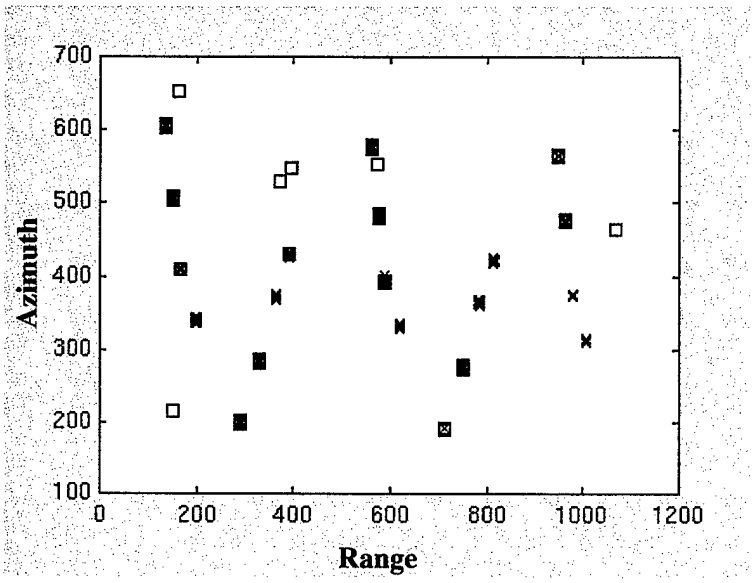

Figure 5.1.4 *The output of the* $x < 20|y|^{3.3} - 0.12$ *detector showing 13 detected targets* (⊠), *6 false alarms* (□), *and 7 missed targets* (×).

Comparing the ultrafine mode result with that of the standard mode (see Figure 5.1.5), there appears to be no significant difference in terms of number of detections or false alarms for the range of target speeds and RCSs examined.

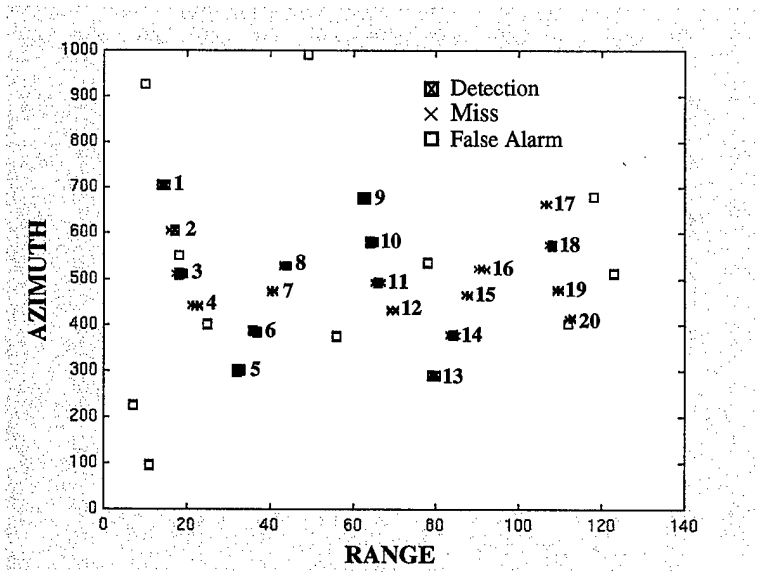

Figure 5.1.5 *Output of "*$x < 10 \cdot |y|^{4.2} - 0.2$*" detector for the standard beam mode, showing 12 detections* (⊠) *(), 7 false alarms* (□), *and 6 missed targets* (×).

The SAR/DPCA processing is also applied to the same signals, and the processor output signal is plotted in Figure 5.1.6, showing the clutter signal suppressed and a few moving targets above the noise floor. Passing the SAR/DPCA data through a cell averaging Constant False Alarm Rate (CFAR) detector, with P_{FA} set at 5×10^{-6}, one obtains the moving target detection plot as shown in Figure 5.1.7

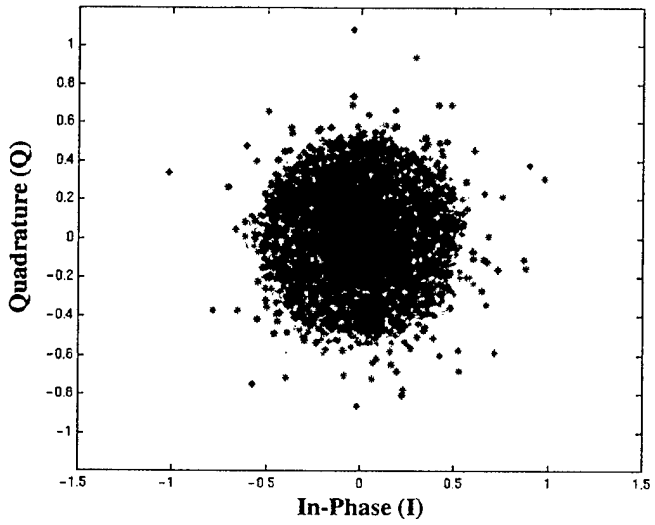

Figure 5.1.6 *Output of the subtractive SAR/DPCA processor, showing clutter signals suppressed and moving target signal above the noise floor.*

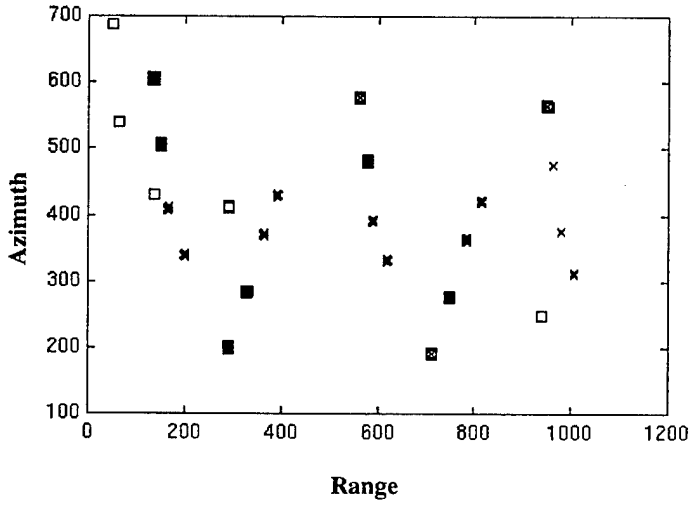

Figure 5.1.7 *Cell-averaging CFAR detector output showing 9 detections (⊠), 11 misses (×), and 5 false alarms (□).*

The result is interesting. The SAR/DPCA processor appears to perform more poorly than the SAR/ATI processor. The SAR/ATI detects 13 out of 20 moving targets compared to 9 out of 20 targets detected for the SAR/DPCA. Its performance also seems to deteriorate with a higher SAR resolution. The difference is quite significant.

5.1.3 Discussions

The results of the ultrafine mode appear to indicate that the performance of the SAR/DPCA processor is poorer than that of the SAR/ATI at the high SAR resolution. One possible explanation for the observed difference is that the noise signal is enhanced in the ultrafine mode due to a larger noise bandwidth. Since the SAR/DPCA processor is a noise-limited detector, for a perfectly suppressed clutter, any increase in the background noise will affect the detector performance. The SAR/ATI detector, on the other hand, is not as sensitive to the increase in the noise background, because it does not rely on clutter suppression to extract moving targets and also because the target signal is squared in the SAR/ATI processing, thus, improving its target-to-noise ratio. In the SAR/ATI, the noise appears in the phase according to $\tan^{-1}\{(S+N)_Q/(S+N)_I\}$, where $S+N$ denotes signal plus noise. The clutter contribution to the target signal is reduced due to a smaller resolution cell size, thus, favoring the clutter-limited SAR/ATI detector.

5.2 Experiment #2: More Low Speeds

The present study is a further investigation of Experiment #1. In that study the initial result indicates that the SAR/DPCA processor performs more poorly than the SAR/ATI processor at the high SAR resolution. The result is, however, based on a single simulation run and may constitute a statistical anomaly. In this study, our goal is to run a few more cases in order to ascertain the observed difference in the processors' performance.

5.2.1 Experimental Definition

Simulations are carried out using the R2 ultrafine mode as the signal generation baseline. Two scenarios are generated. The first one is exactly the same as the Section 5.1 run with only random number generation seeds changed. Scenario 2 has the same simulation parameters as Scenario 1, except target speeds are changed from 12-54 km/h to 15-24 km/h. This range of speeds is expected to accentuate the difference in performance observed between the two processors, because targets at these speeds are usually detected by the SAR/ATI but not by the SAR/DPCA as observed in Experiment #1. The radar system parameters used for the two scenarios are shown in Table 5.1.1.

The target parameters for Scenario 1 are summarized in Table 5.2.1 and for Scenario 2 in Table 5.2.2. There are 20 targets moving either eastward or westward. The targets' initial positions in the land patch for Scenarios 1 and 2 are shown in Figures 5.1.1 and 5.2.1, respectively. The detailed signal generation parameters for this experiment are listed in Appendix B.

Table 5.2.1 *Target Parameters: Scenario 1*

Target Number	RCS (m^2)	Speed (km/h)
1	45	54 (east)
2	45	36 (east)
3	45	18 (east)
4	45	12 (east)
5	40	54 (west)
6	40	36 (west)
7	40	18 (west)
8	40	12 (west)
9	35	54 (east)
10	35	36 (east)
11	35	18 (east)
12	35	12 (east)
13	30	54 (west)
14	30	36 (west)
15	30	18 (west)
16	30	12 (west)
17	20	54 (east)
18	20	36 (east)
19	20	18 (east)
20	20	12 (east)

Table 5.2.2 *Target Parameters: Scenario 2*

Target Number	RCS (m^2)	Speed (km/h)
1	45	24 (east)
2	45	21 (east)
3	45	18 (east)
4	45	15 (east)
5	40	24 (west)
6	40	21 (west)
7	40	18 (west)
8	40	15 (west)
9	35	24 (east)
10	35	21 (east)
11	35	18 (east)
12	35	15 (east)
13	30	24 (west)
14	30	21 (west)
15	30	18 (west)
16	30	15 (west)
17	20	24 (east)
18	20	21 (east)
19	20	18 (east)
20	20	15 (east)

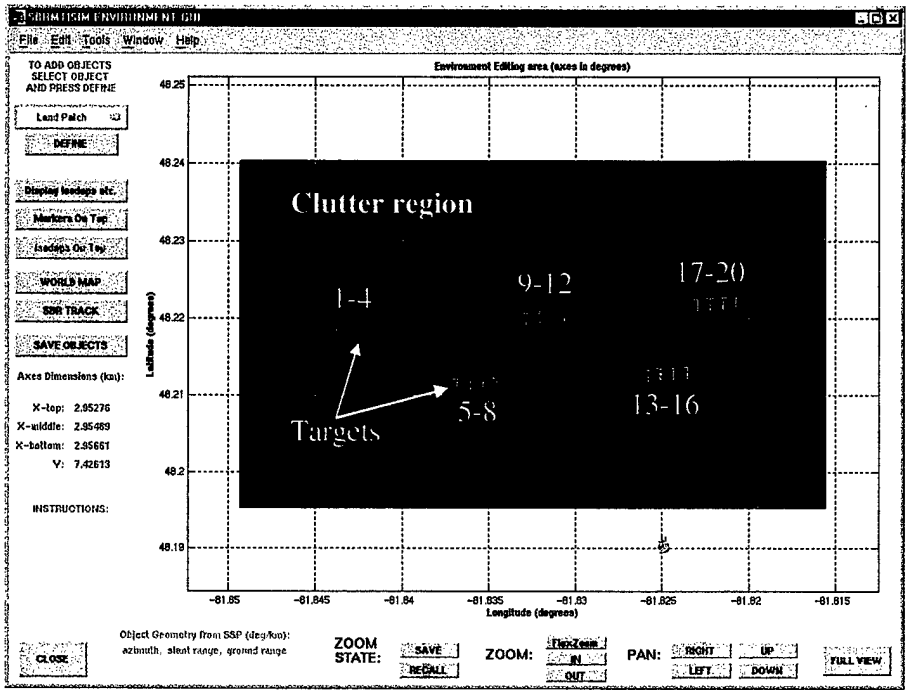

Figure 5.2.1 *Environment definition for Scenario 2 (filename "Sep13_00#7") showing 20 moving targets in a land patch*

5.2.2 Results

(a) Scenario 1:

The processed complex signals and the GMTI detector outputs for Scenario 1 from the two processors are plotted in Figure 5.2.2. The radar signals are generated using a set of random number generator seeds that are different from those of the Section 5.1 run (filename "Aug17_00#1"). Again, the result shows that the SAR/ATI is a superior approach than the SAR/DPCA at the high SAR resolution. For the SAR/ATI, 13 out of 20 targets are detected compared to 10 out of 20 detected for the SAR/DPCA. The experiment is repeated again using another set of random number generator seeds, and the result is again consistent with those of the two previous runs.

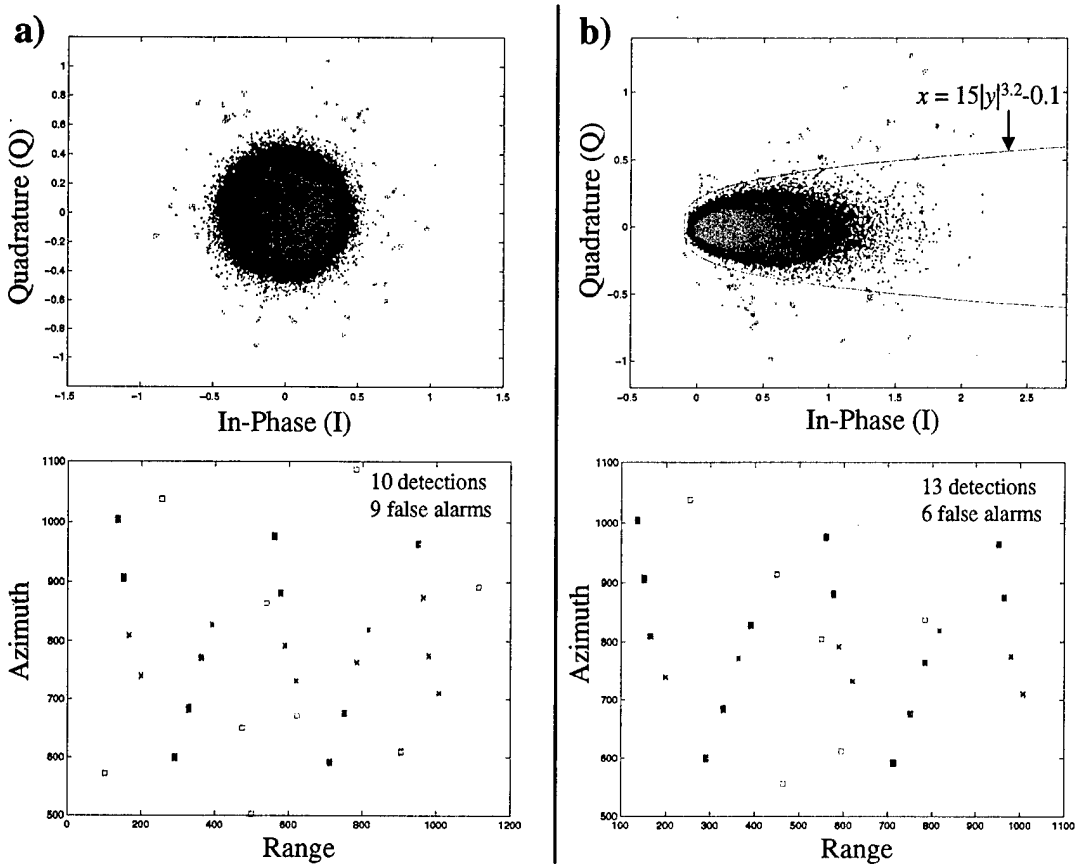

Figure 5.2.2 *Complex signals and detector outputs from (a) the SAR/DPCA processor and (b) the SAR/ATI processor: Scenario 1 and filename "Sep13_00#1"*

(b) Scenario 2:

The results from Scenario 1 show that the targets with velocities in the vicinity of 20 km/h are particularly interesting, because these are the ones that are often missed by the SAR/DPCA but detected by the SAR/ATI. So in order to highlight the difference observed in the two detectors' performance, we have set the target speeds to 15 to 24 km/h. The result from one of Scenario 2 runs is plotted in Figure 5.2.3.

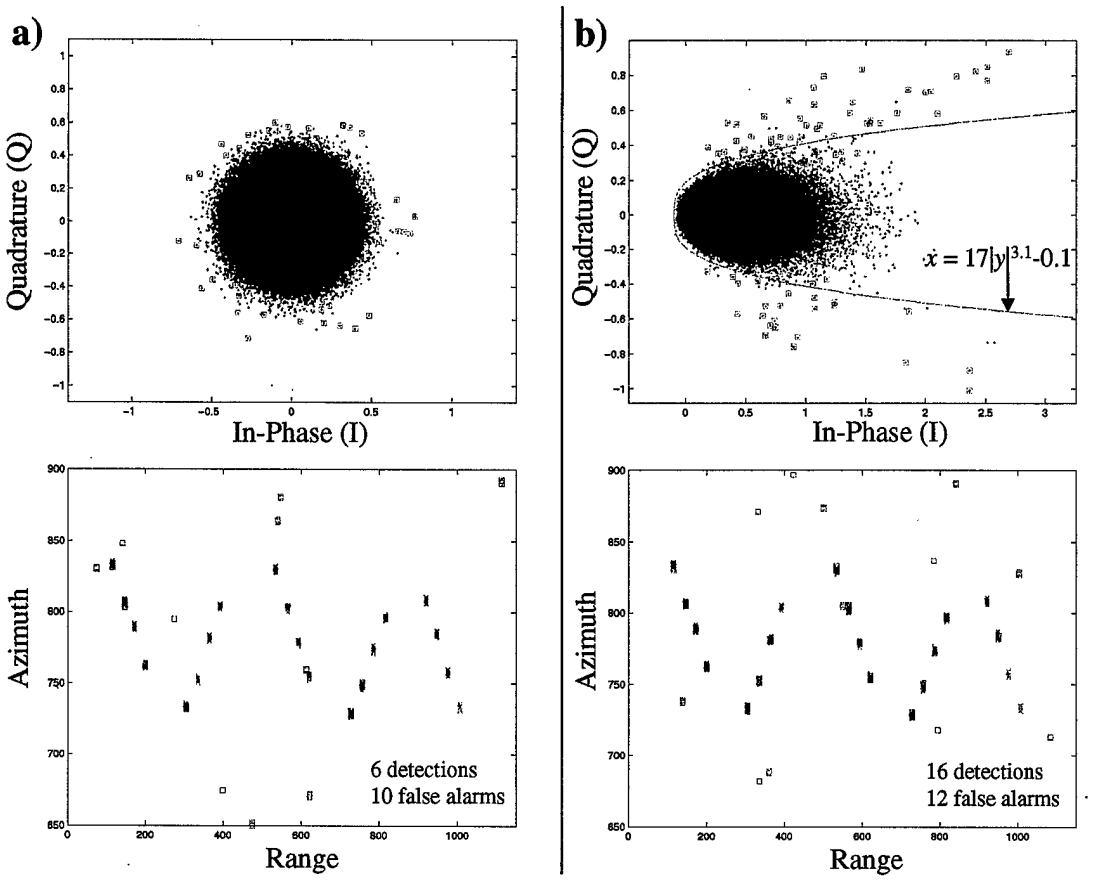

Figure 5.2.3 *Complex signals and detector outputs from (a) the SAR/DPCA processor and (b) the SAR/ATI processor: Scenario 2 and filename "Sep13_00#8"*

The difference in the processors' performance is indeed accentuated. For the SAR/ATI, 16 out of 20 targets are detected compared to 6 out of 20 detected for the SAR/DPCA. The difference is truly significant. But in order to ascertain the observed result, we carry out another Scenario 2 run using a different set of random number generator seeds. The result agrees with the previous run, further supporting the conclusion. The results from the five simulation runs, including the one from Section 5.1, are summarized in Table 5.2.3.

Table 5.2.3 *Summary of SAR/ATI and SAR/DPCA Performances*

FILENAME	PROCESSOR TYPE	DETECTIONS	FALSE ALARMS
A. Scenario 1 (different signal generation seeds for each run)			
Aug17_00#1	ATI	13	6
	SAR DPCA	9 9	1 5
Sep13_00#1	ATI	13	6
	SAR DPCA	9 10	4 9
Sep13_00#2	ATI	15	11
	SAR DPCA	13	11
B. Scenario 2 (different signal generation seeds for each run)			
Sep13_00#7	ATI	15 16	5 13
	SAR DPCA	7 8 8	3 8 20
Sep13_00#8	ATI	16 14	12 2
	SAR DPCA	5 6 7	4 10 17

5.2.3 Discussions

We have conclusively shown that the SAR/ATI processor is a superior ground moving target indicator than the SAR/DPCA processor at the high SAR resolution mode, particularly for targets moving at relatively slow speeds (i.e. without significant matched-filter mismatch and image smearing).

5.3 Experiment #3: High Speeds

In Section 5.2 it is concluded that the performance of the SAR/ATI processor is better than the SAR/DPCA processor at the high SAR resolution. This is based on the results of several simulation runs at relatively low target speeds (12 to 54 km/h). In this study, one would like to investigate whether the same performance superiority of the SAR/ATI processor is also observed at high target velocities (> 100 km/h).

5.3.1 Experimental Definition

The ultrafine mode is again the baseline for this study. Twenty moving targets with various RCSs and velocities are generated. The experiment, which we will call Scenario 3, consists of twenty targets with speeds ranging from 100 km/h to 130 km/h and RCSs from 20 m^2 to 45 m^2. These targets are initially positioned in a land patch as shown in Figure 5.3.1. The simulation parameters are exactly the same as those of the Section 2.1 run, except for the higher target speeds. The target parameters are summarized in Table 5.3.1 and the detailed simulation data are listed in Appendix C.

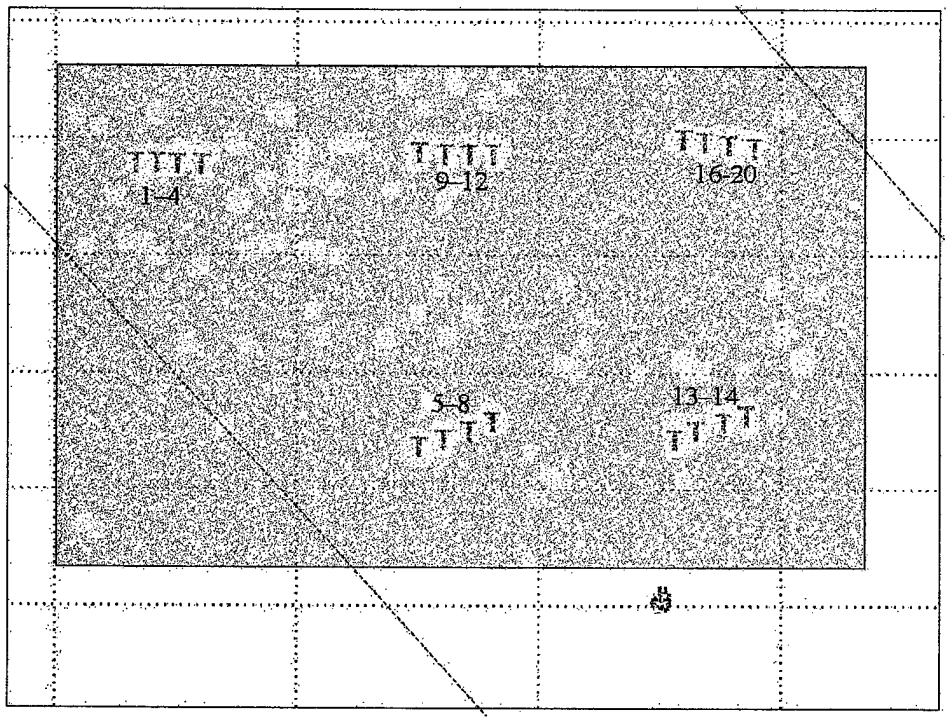

Figure 5.3.1 *Environment definition for 20 targets and a clutter background: Scenario 3*

Table 5.3.1 *Target Parameters: Scenario 3*

Target Number	RCS (m^2)	Speed (km/h)
1	45	130 (east)
2	45	120 (east)
3	45	110 (east)
4	45	100 (east)
5	40	130 (west)
6	40	120 (west)
7	40	110 (west)
8	40	100 (west)
9	35	130 (east)
10	35	120 (east)
11	35	110 (east)
12	35	100 (east)
13	30	130 (west)
14	30	120 (west)
15	30	110 (west)
16	30	100 (west)
17	20	130 (east)
18	20	120 (east)
19	20	110 (east)
20	20	100 (east)

5.3.2 Results:

The generated signals from the two radar channels are processed using the two GMTI processing approaches. The output of the SAR/DPCA processor is plotted in a complex plane as shown in Figure 5.3.2. The clutter signal is suppressed with the DPCA filter and a few targets are clearly seen above the noise floor.

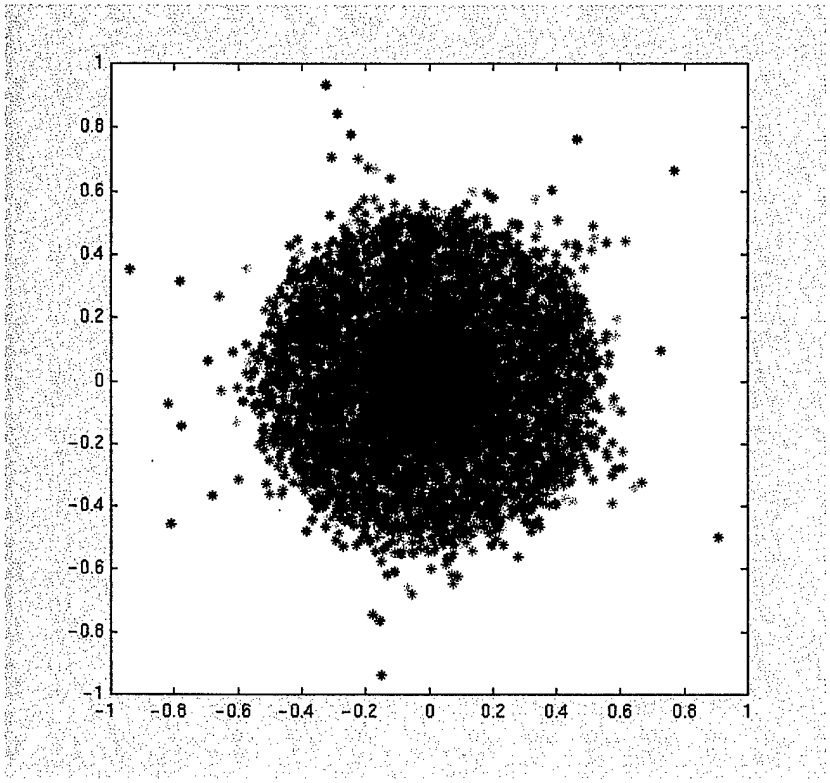

Figure 5.3.2 *SAR/DPCA processor output with clutter suppressed and a few targets above the noise floor: Scenario 3*

Using a cell-averaging CFAR detector to extract the targets from the noise background yields a detection plot as shown in Figure 5.3.3. Nine out of twenty moving targets are detected with 10 false alarms. All of the targets at 130 km/h are missed and only one target at 120 km/h is detected. Targets at the lowest speed (100 km/h) are all detected. As expected, the targets with the highest radial speed are least likely to be detected, since the stationary-terrain matched filter is poorly matched to these targets. This has the effect of reducing the targets' signal and smearing their image.

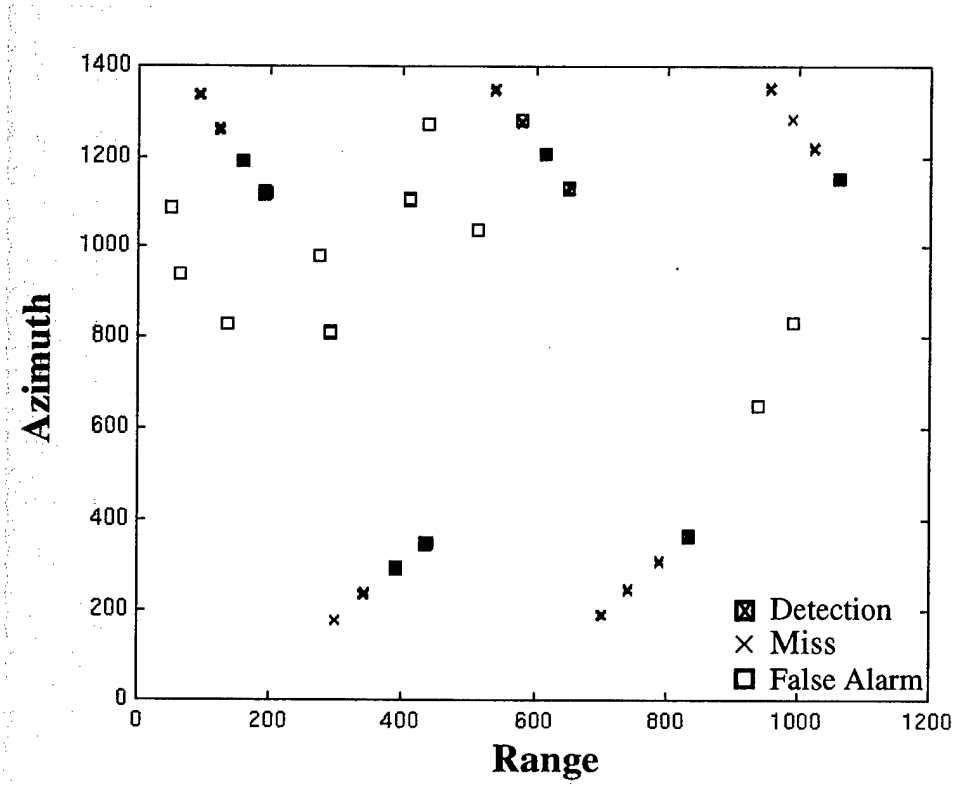

Figure 5.3.3 *Output of the CFAR detector: Scenario 3*

The complex signal output from the SAR/ATI processor is also plotted in Figure 5.3.4. The "$x < 3\ |y|^2 - 0.075$" detector is used to extract moving targets from the clutter. The output of the detector is shown in Figure 5.3.5. The result is very similar to that of the SAR/DPCA processor. There are 9 out of 20 targets detected with 7 false alarms. Again, all 130 km/h targets are missed and only one 120 km/h target is detected. Similarly, all 100 km/h targets are detected.

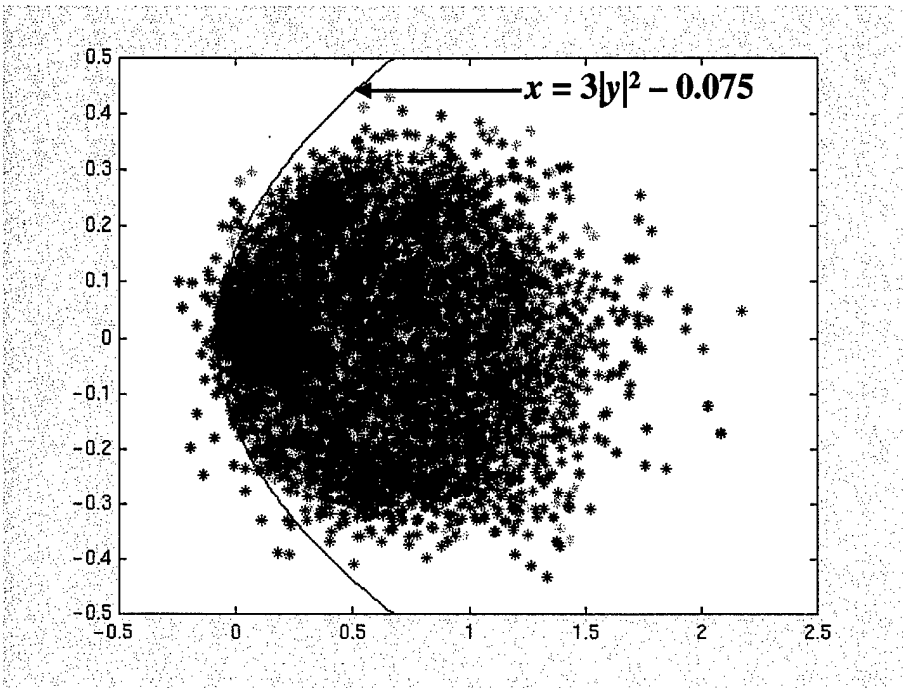

Figure 5.3.4 *ATI processed signal plotted in a complex plane. An "$x = 3\,|y|^2 - 0.075$" detector is used to extract moving targets from the clutter background.*

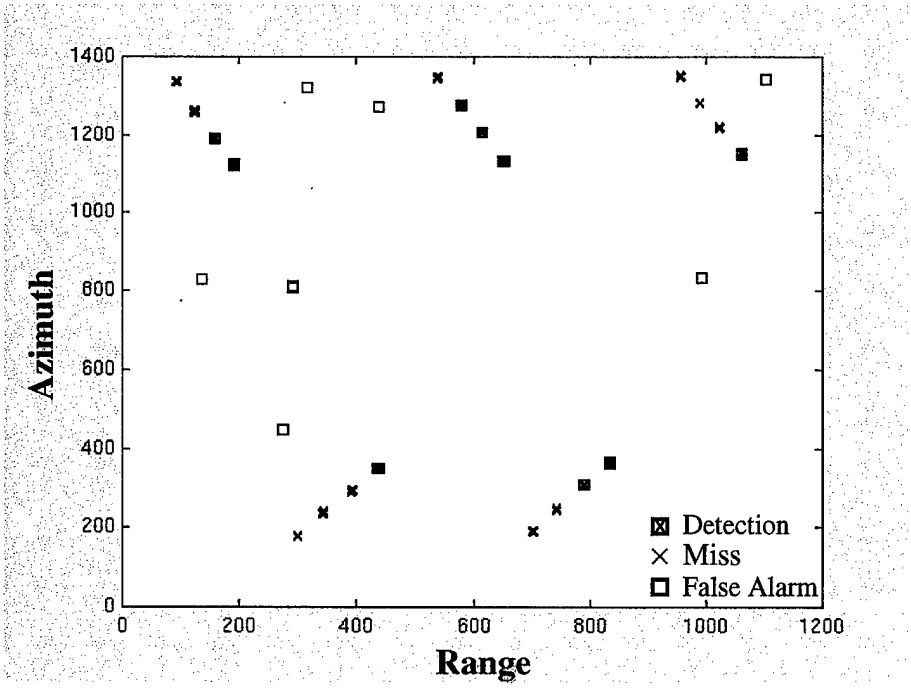

Figure 5.3.5 *The output of the "$x = 3\,|y|^2 - 0.075$" detector.*

5.3.3 Discussions

Unlike the low target speed case, the two GMTI processing approaches do not show a noticeable difference in their performance when detecting high-speed targets. This is interesting since the SAR/ATI clearly demonstrates GMTI superiority over the SAR/DPCA at low target speeds as shown in Sections 5.1 and 5.2. The present result appears to indicate that the velocity mismatch between the matched filter and the moving targets may have played an important role in influencing the two processors' ability to detect high-speed targets. The target signals may have been reduced significantly, due to the poorly matched filter, to the extent that the both processors are now noise-limited. This filter mismatch effect is further explored in the next sub-section.

5.4 Experiment #4: Velocity-Offset Matched Filter

To illustrate the effect of the matched filter mismatching the high-speeds targets, discussed in the previous sub-section, we carry out a fourth experiment in order to evaluate the effect of incorporating a velocity-offset in the terrain matched filter.

5.4.1 Experimental Definition

In order to reduce the signal generation time, the R2 standard mode is used for this experiment. The low resolution mode is sufficient for the purpose of this study, because we are mainly interested in the general performance of the SAR/ATI processor as a function of velocity matching of the matched filter to the targets. The simulation parameters are the same as those of the Section 5.3 run, except for the standard beam mode. The targets have ground speeds ranging from 100 to 130 km/h and RCSs from 20 to 45 m^2. Their directions are either east or west. The background clutter has a mean clutter cross-section of 0.1 m^2/m^2 and a spectral width of 0.1 m/s.

5.4.2 Results

(a) Terrain-Matched Filter:

Using a matched filter for the stationary terrain, the resulting complex interferogram from the SAR/ATI processor is as shown in Fig. 5.4.1.

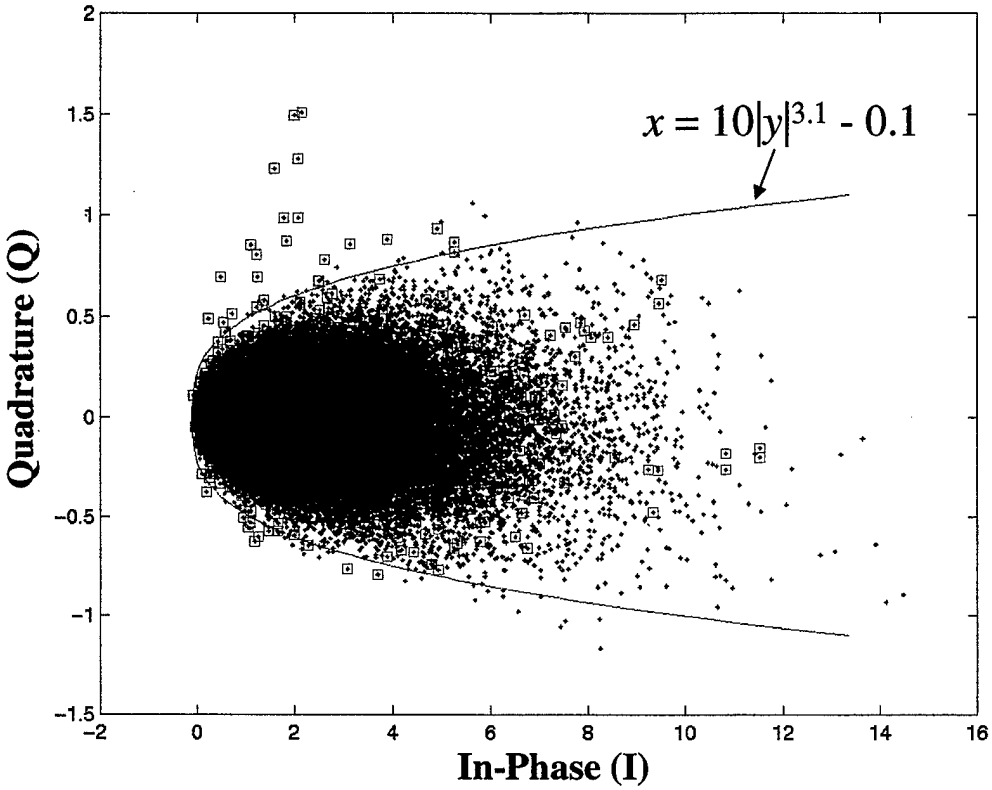

Figure 5.4.1 *Complex interferogram showing the clutter signal in blue dots and the moving target signals in red squares. Processed by a stationary terrain matched filter.*

As can be seen in the figure, the moving targets' signal energy falling within the stationary terrain frequency spectrum is fully captured by the matched filter and is also centered around the zero phase axis as the clutter's signal. This portion of the targets' signal is indistinguishable from that of the clutter. Some portion of the targets' signal has phase angles that are large enough to bring them out of the clutter region. These can then be detected by a well designed detector such as "$x < 10|y|^{3.1} - 0.1$", as shown in the figure. However, due to the high speeds of these targets, a major portion of their energy is not captured, thus, making their detection much more difficult. The output of the "$x < 10|y|^{3.1} - 0.1$" detector is plotted in Figure 5.4.2.

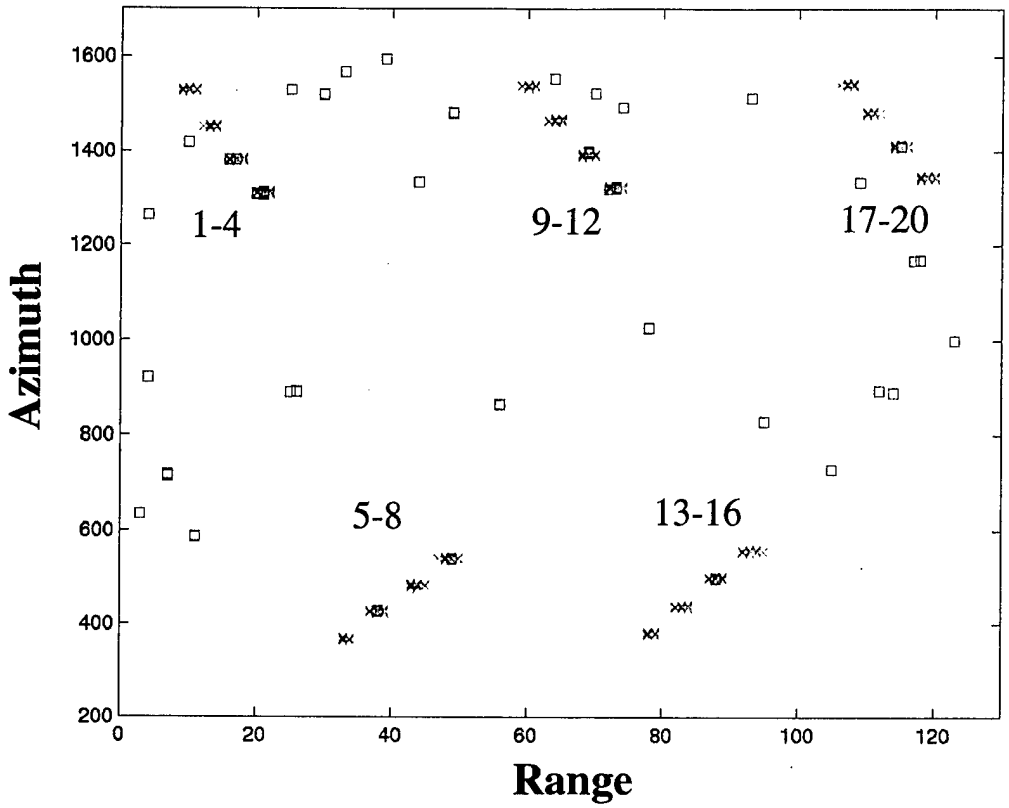

Figure 5.4.2 *Output of the "$x < 10|y|^{3.1} - 0.1$" detector: ⊠ target detected, □ false alarm, and × target missed.*

Only 8 out of 20 targets are detected using this matched filter. All the 130 km/h targets (#1, #5, #9, #13, and #17) are missed and only one 120 km/h target (#6) is detected. This result is very similar to that of the high resolution mode described in the previous sub-section. As we have stated earlier, the result is consistent with the fact that the terrain matched filter is not well matched to the moving targets with high radial speeds.

(b) Velocity-Offset Matched Filter:

In order to see more clearly what the matched filter is doing to the targets' signal, a "targets-only" scenario is also generated and a matched filter with or without a velocity-offset is applied to the generated signal. In this run, the clutter and the thermal noise are removed from the synthetic scene, allowing only the targets' signal to be processed. When a terrain-matched filter is applied to the targets-only raw data, the resulting complex signal interferogram is as shown in Figure 5.4.3. As expected, the target signals are clean with well-defined phase angles. Depending on the moving

targets' direction of travel with respect to the sensor, the phase angles are either positive or negative.

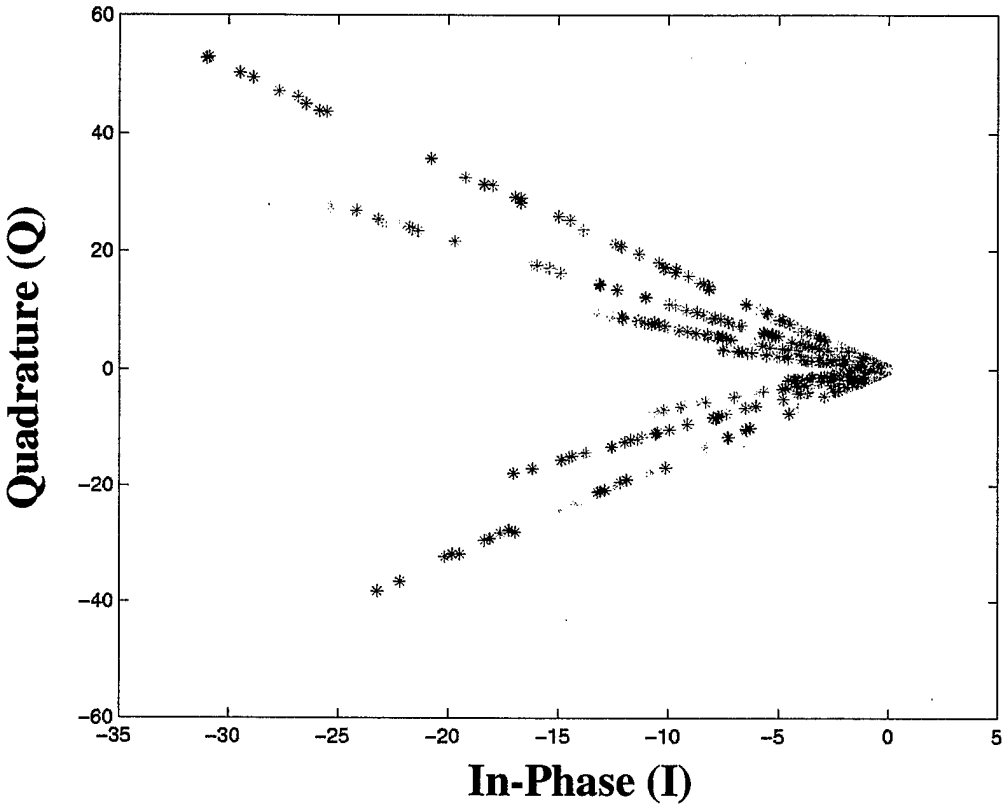

Figure 5.4.3 *Complex signal interferogram for the "targets-only" case, processed by a stationary terrain matched filter.*

As can be noted in the figure, the amplitude of the signals decreases with an increasing phase angle (i.e., with an increasing radial velocity). The result is again consistent with a matched filter that is increasingly mismatched to the targets that have increasingly larger radial speeds.

When the same raw data are processed with a velocity-offset (+100 km/h) matched filter, the resulting complex interferogram is as shown in Figure 5.4.4. The signals from targets with positive radial velocities are enhanced, whereas those with negative radial speeds are completely suppressed. The enhancement is particularly pronounced for +110 km/h targets, which have a radial component of about +90 km/h. So the filter is more matched to these targets than to all the other lower speed targets.

Applying this velocity-offset matched filter to the full scenario case, which includes the clutter and the thermal noise, one obtains a complex signal interferogram as shown in Figure 5.4.5.

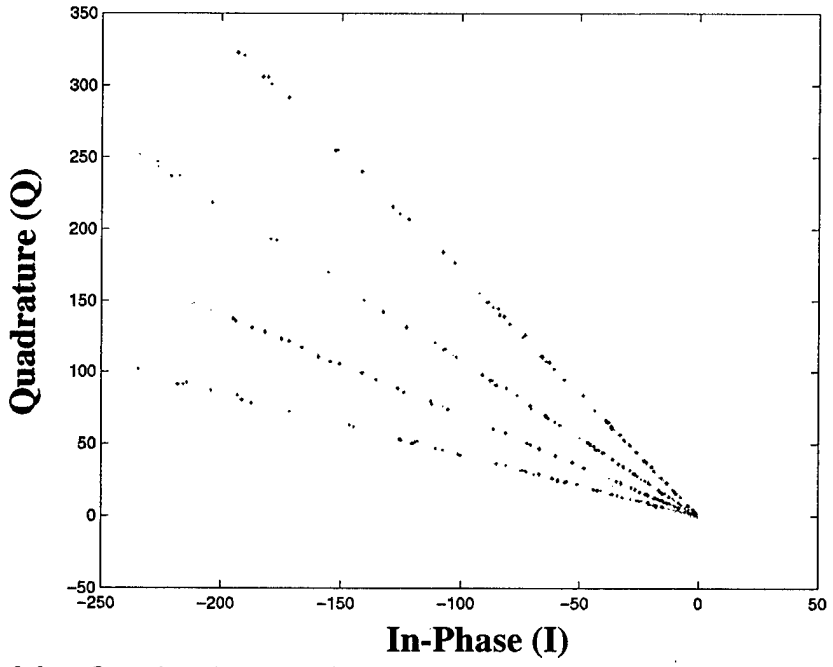

Figure 5.4.4 *Complex signal interferogram of the "targets-only" case, processed by a +100 km/h velocity-offset matched filter.*

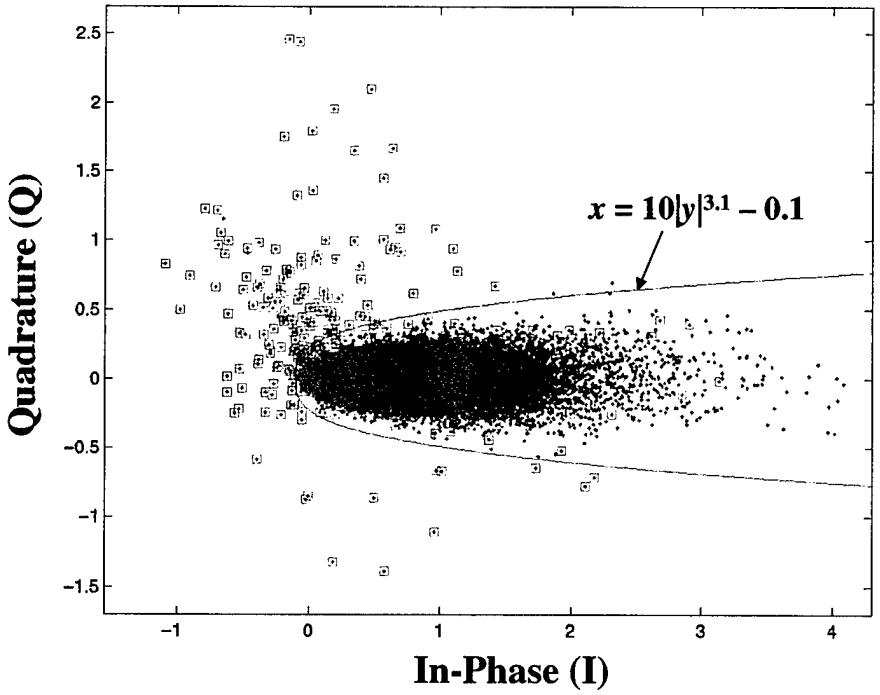

Figure 5.4.5 *Complex signal interferogram of the full scenario showing the clutter signal in blue dots and the moving target signal in red squares. Processed with a +100 km/h velocity-offset matched filter.*

The positive velocity targets are clearly enhanced compared to those of Figure 5.4.1, with the clutter region significantly suppressed. One should note that even though the filter is matched to the moving targets, the clutter signal is still centered around the zero-phase axis in the complex plane. This is because the two channels' data are processed with the same velocity-offset matched filter, followed by the conjugate multiplication operation. The latter operation nulls the phase angle of any stationary object in the scene, but any change in the scene will appear as a phase shift in the complex plane.

Applying the same "$x < 10|y|^{3.1} - 0.1$" detector on the reprocessed signal, one obtains a detection plot as shown in Figure 5.4.6. All the positive velocity targets are now detected but all negative velocity targets are missed. Also, the number of false alarms is significantly reduced (1 false alarm compared to previously 13 false alarms).

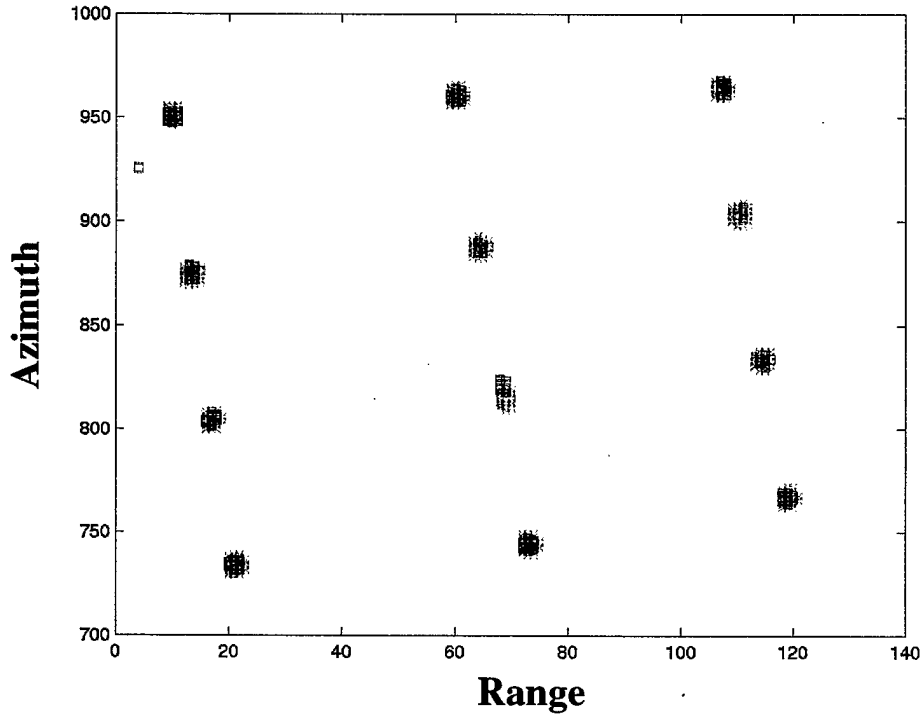

Figure 5.4.6 *Output of the "$x < 10|y|^{3.1} - 0.1$" detector: ⊠ target detected, □ false alarm, and × target missed. Reprocessing of the full scenario case using a positive velocity-offset matched filter.*

Similarly, the reprocessing was done for the same raw data using a −100 km/h velocity-offset matched filter. The results are plotted in Figures 5.4.7 to 5.4.9. The situation is exactly reversed for the negative velocity-offset processing. The negative velocity targets are now enhanced and the positive ones suppressed; see Figures 5.4.7 and 5.4.8. The clutter is similarly reduced (Figure 5.4.8). All negative velocity targets

are detected (Figure 5.4.9) without any difficulty using the same detector from the two previous cases. Also, only a few alarms are observed.

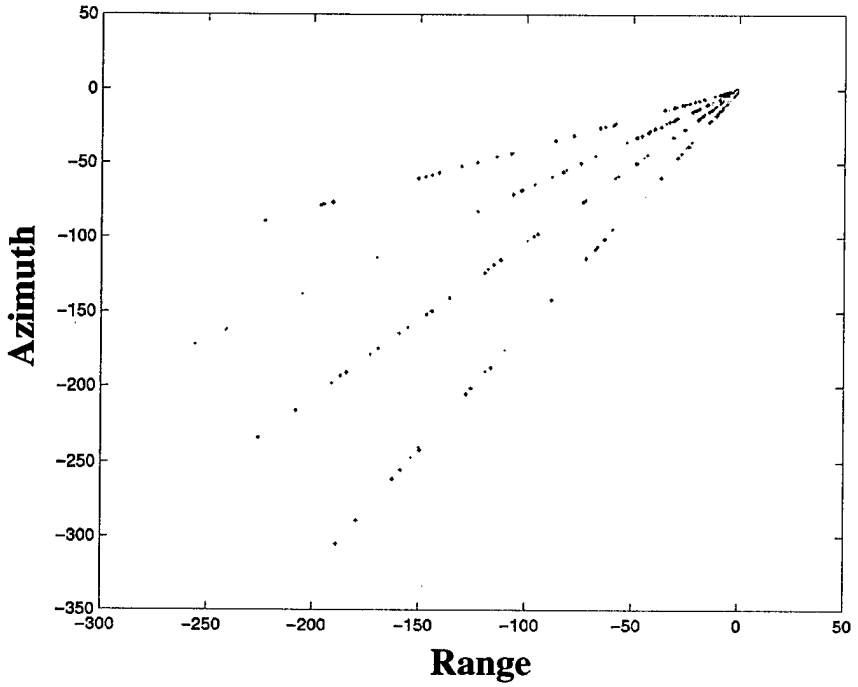

Figure 5.4.7 *Complex signal interferogram for the "targets-only" case, processed with a −100 km/h velocity-offset matched filter.*

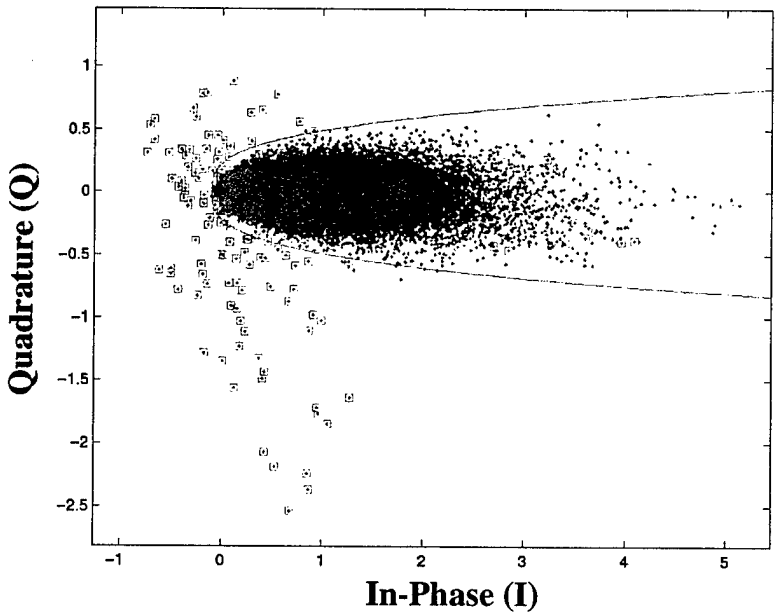

Figure 5.4.8 *Complex signal interferogram showing the clutter signal in blue dots and the moving target signal in red squares. Reprocessing of the full scenario case using a −100 km/h velocity-offset matched filter.*

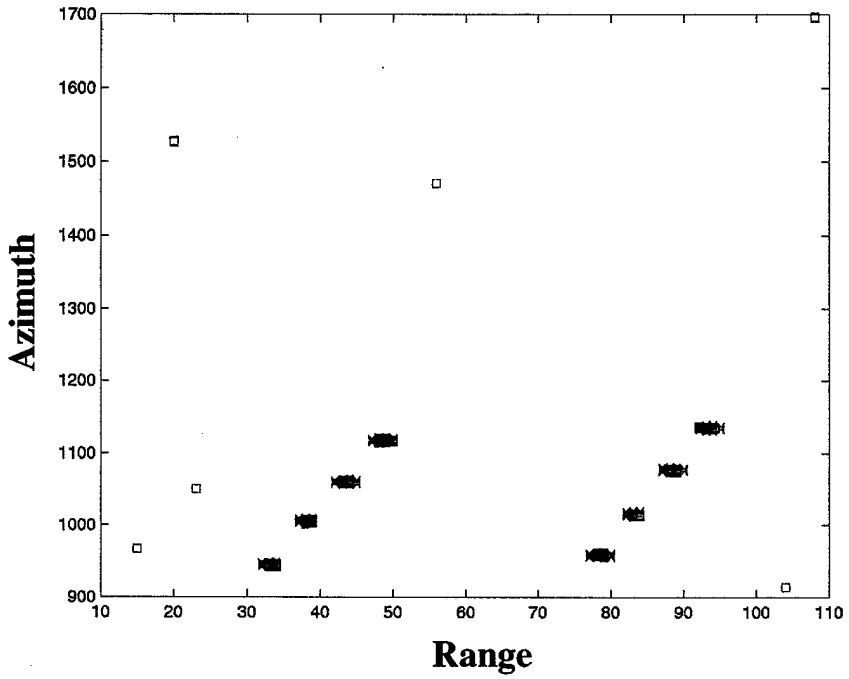

Figure 5.4.9 *Output of the "$x < 10|y|^{3.1} - 0.1$" detector: ⊠ target detected, □ false alarm, and × target missed. Reprocessing of the full scenario case using a positive velocity-offset matched filter.*

5.4.3 Discussions

The moving target enhancement is clearly demonstrated by reprocessing the raw data using a velocity-offset matched filter. It is also shown that it is not necessary to have perfect matching between the matched filter and the targets to significantly improve their detectability. This suggests that one may choose a "best" velocity offset for a range of velocities of interest. Once the targets are identified, their velocities can then be computed from their phase information and the clutter content surrounding these targets. A systematic moving target search scheme may also be devised based on this velocity-offset technique.

6. Conclusions

Two GMTI processing approaches are currently being considered for Canada's RADARSAT2 MODEX mode. One makes use of the classical SAR/DPCA clutter cancellation technique to provide sub-clutter visibility for dim moving objects. The other is based on the along-track SAR interferometer (SAR/ATI) technique, where amplitude and phase information of the targets are exploited to allow their extraction from the clutter background. The performance of each processor is examined for the RADARSAT2 ultrafine beam mode. The study focuses on the influence of SAR resolution on the processor performance.

Results clearly demonstrate that, at high SAR resolution, the SAR/ATI processor performs better than the SAR/DPCA processor in its ability to detect dim slowly moving targets. Possible reasons for the observed difference in the processor performance include an enhanced noise signal due to a larger noise bandwidth and a reduced clutter contribution to the target signal due to a smaller resolution cell size at the high-resolution mode. The processors' performance is also evaluated for high-speed targets (> 100 km/h). Unlike the low speed case, the two processors do not show a noticeable difference in their performance when the terrain-matched filter is used.

References

[1] Coe, D.J., White, R.G., " Moving Target Detection in SAR Imagery: Experimental Results," IEEE International Radar Conference, 1995, 644-649.

[2] Stockburger, E.F., Held, D.N., "Interferometric Moving Ground Target Imaging," IEEE International Radar Conference, 1995, 438-443.

[3] Ender, J.H.G., "Space-Time Processing for Multichannel Synthetic Aperture Radar," Electronics & Communication Engineering Journal, 11, 1999, 29-38.

[4] Yadin, E., "Evaluation of Noise and Clutter Induced Relocation Error in SAR MTI," IEEE International Radar Conference, 1995, 650-655.

[5] Livingstone, C., "The Addition of MTI Modes to Commercial SAR Satellites," Proc. of 10th CASI Conference on Astronautics, Ottawa, Canada, October 26-28, 1998.

[6] Luscombe, A., "The Radarsat Project," IEEE Canadian Review, Fall 1995.

[7] S. Chiu, C. Livingstone, T. Knight, and I. Sikaneta, "Computer Simulations of Canada's RADARSAT 2 GMTI," NATO SET Conference, Samos, Greece (16-18 October 2000).

Appendix A: Signal Generation Parameters (Section 2.1)

Filename: Aug17_00#1 (Scenario 1)

Platform: SBR
Orbit: altitude (km) 792, inclination (deg) 98.6
Initial sub satellite point: longitude (deg) -90, latitude (deg) 47
Initial SBR direction: NORTH
peak power (watts): 5120
carrier frequency (GHz): 5.4
expanded pulse width (usec): 42
pulse bandwidth (MHz): 100
burst length (sec): 0.75
noise temperature (K): 1893
prf (Hz): 1988.3
A/D sampling rate (MHz): 112.6
waveform modulation: LFM
model receiver: yes
IF bandwidth (MHz): 112
IF filter type: Butterworth
IF filter order: 8
IF centre frequency (MHz): 1500
channel to channel mismatch (dB): -50
A/D quantization level (dB): -100
number of A/D bits: 8
number of Mismatch Ripples: 4
PRI compensation: no
ZRT compensation: no
radar system loss (dB): 0
spotlighting: no
fill pulse duration (ms): 0
model phase noise: no

thermal noise seed: 123456789
antenna seed: 232323232
clutter seed: 777777777
target seed: 567567567
jammer seed: 372372372
motion seed: 952952952
channel response seed: 101001000
available memory (MB): 800
brute-force pulse summation: no
pulse oversampling factor: 11
brute-force antenna patterns: no
pattern oversampling factor: 30

array type: phased_array
number of receive apertures: 2
grid spacing along x (m): 0.046
grid spacing along y (m): 0.046
random sidelobe level (dB): -50
physical shape: rectangular

TRANSMIT APERTURE:
x-width (m): 15
y-width (m): 0.75
x position (m): 0
y position (m): 0
x taper: uniform
y taper: uniform

RECEIVE APERTURE 1:
x-width (m): 7.5
y-width (m): 0.75
x position (m): -3.75
y position (m): 0
x taper: uniform
y taper: taylor
y sidelobe level (dB): -40

RECEIVE APERTURE 2:
x-width (m): 7.5
y-width (m): 0.75
x position (m): 3.75
y position (m): 0
x taper: uniform
y taper: taylor
y sidelobe level (dB): -40

SWATH longitude: -81.8249
swath latitude: 48.1904
swath range width (m): 1500

MECH BORESIGHT longitude: -81.8249
mech boresight latitude: 48.1904
mech boresight frd azimuth: 87.481
mech boresight elevation: 37.2849

ELEC BORESIGHT longitude: -81.8249
elec boresight latitude: 48.1904
elec boresight frd azimuth: 87.481
elec boresight elevation: 37.2849

TARGET number: 20
type: Wheeled
longitude (deg): -81.8207
latitude (deg): 48.2218

backscatter statistics: fixed
mean target RCS (m^2): 20
speed (km/h): 12
heading East of North (deg): 90
spectral width (m/s): 0

TARGET number: 19
type: Wheeled
longitude (deg): -81.8213
latitude (deg): 48.2212
backscatter statistics: fixed
mean target RCS (m^2): 20
speed (km/h): 18
heading East of North (deg): 90
spectral width (m/s): 0

TARGET number: 18
type: Wheeled
longitude (deg): -81.822
latitude (deg): 48.2223
backscatter statistics: fixed
mean target RCS (m^2): 20
speed (km/h): 36
heading East of North (deg): 90
spectral width (m/s): 0

TARGET number: 17
type: Wheeled
longitude (deg): -81.8227
latitude (deg): 48.2237
backscatter statistics: fixed
mean target RCS (m^2): 20
speed (km/h): 54
heading East of North (deg): 90
spectral width (m/s): 0

TARGET number: 16
type: Wheeled
longitude (deg): -81.8235
latitude (deg): 48.2126
backscatter statistics: fixed
mean target RCS (m^2): 30
speed (km/h): 12
heading East of North (deg): -90
spectral width (m/s): 0

TARGET number: 15
type: Wheeled
longitude (deg): -81.8244
latitude (deg): 48.2128
backscatter statistics: fixed
mean target RCS (m^2): 30
speed (km/h): 18
heading East of North (deg): -90
spectral width (m/s): 0

TARGET number: 14
type: Wheeled
longitude (deg): -81.8249
latitude (deg): 48.2112
backscatter statistics: fixed
mean target RCS (m^2): 30
speed (km/h): 36
heading East of North (deg): -90
spectral width (m/s): 0

TARGET number: 13
type: Wheeled
longitude (deg): -81.8255
latitude (deg): 48.2095
backscatter statistics: fixed
mean target RCS (m^2): 30
speed (km/h): 54
heading East of North (deg): -90
spectral width (m/s): 0

TARGET number: 12
type: Wheeled
longitude (deg): -81.8306
latitude (deg): 48.2201
backscatter statistics: fixed
mean target RCS (m^2): 35
speed (km/h): 12
heading East of North (deg): 90
spectral width (m/s): 0

TARGET number: 11
type: Wheeled
longitude (deg): -81.8313
latitude (deg): 48.2196
backscatter statistics: fixed
mean target RCS (m^2): 35
speed (km/h): 18
heading East of North (deg): 90
spectral width (m/s): 0

TARGET number: 10
type: Wheeled
longitude (deg): -81.832
latitude (deg): 48.221
backscatter statistics: fixed
mean target RCS (m^2): 35
speed (km/h): 36
heading East of North (deg): 90
spectral width (m/s): 0

TARGET number: 9
type: Wheeled
longitude (deg): -81.8327
latitude (deg): 48.2222
backscatter statistics: fixed
mean target RCS (m^2): 35
speed (km/h): 54
heading East of North (deg): 90
spectral width (m/s): 0

TARGET number: 8
type: Wheeled
longitude (deg): -81.8345
latitude (deg): 48.2112
backscatter statistics: fixed
mean target RCS (m^2): 40
speed (km/h): 12
heading East of North (deg): -90
spectral width (m/s): 0

TARGET number: 7
type: Wheeled
longitude (deg): -81.8353
latitude (deg): 48.2114
backscatter statistics: fixed
mean target RCS (m^2): 40
speed (km/h): 18
heading East of North (deg): -90
spectral width (m/s): 0

TARGET number: 6
type: Wheeled
longitude (deg): -81.8358
latitude (deg): 48.2098
backscatter statistics: fixed
mean target RCS (m^2): 40
speed (km/h): 36
heading East of North (deg): -90
spectral width (m/s): 0

TARGET number: 5
type: Wheeled
longitude (deg): -81.8364
latitude (deg): 48.2081
backscatter statistics: fixed
mean target RCS (m^2): 40
speed (km/h): 54
heading East of North (deg): -90
spectral width (m/s): 0

TARGET number: 4
type: Wheeled
longitude (deg): -81.8415
latitude (deg): 48.2187
backscatter statistics: fixed
mean target RCS (m^2): 45
speed (km/h): 12
heading East of North (deg): 90
spectral width (m/s): 0

TARGET number: 3
type: Wheeled
longitude (deg): -81.8422
latitude (deg): 48.2179
backscatter statistics: fixed
mean target RCS (m^2): 45
speed (km/h): 18
heading East of North (deg): 90
spectral width (m/s): 0

TARGET number: 2
type: Wheeled
longitude (deg): -81.8429
latitude (deg): 48.2191
backscatter statistics: fixed
mean target RCS (m^2): 45
speed (km/h): 36
heading East of North (deg): 90
spectral width (m/s): 0

TARGET number: 1
type: Wheeled
longitude (deg): -81.8436
latitude (deg): 48.2202
backscatter statistics: fixed
mean target RCS (m^2): 45
speed (km/h): 54
heading East of North (deg): 90
spectral width (m/s): 0

PATCH number: 1
type: land
centre longitude (deg): -81.8324
centre latitude (deg): 48.2178
long-size (km): 2.5
lat-size (km): 5
along-range scatterer spacing (m): 2
cross-range scatterer spacing (m): 4
backscatter statistics: rayleigh
mean clutter cross-section (m^2/m^2): 0.1
spectral width (m/s): 0.1

SIGNAL PROCESSING PARAMETERS
Baseline: SAR
rx channel numbers: 1:2
pulse compression: yes

pulse doppler window: Hamming
pulse compression window: Hamming
SAR Pulses Used: 1:1490

SAR Replica Length: 700
BAQ bits: off

Appendix B: Signal Generation Parameters (Section 2.2)

Filename: Sep13_00#1 (Scenario 1)
thermal noise seed: 987654321
antenna seed: 323232323
clutter seed: 666666666
target seed: 765765765
jammer seed: 237237237
motion seed: 259259259
channel response seed: 101001011
available memory (MB): 800
brute-force pulse summation: no
pulse oversampling factor: 11
brute-force antenna patterns: no
pattern oversampling factor: 30

Filename: Sep13_00#2 (Scenario 1)
thermal noise seed: 121212121
antenna seed: 321321321
clutter seed: 999999999
target seed: 365365365
jammer seed: 98123765
motion seed: 123454321
channel response seed: 746132469
available memory (MB): 800
brute-force pulse summation: no
pulse oversampling factor: 11
brute-force antenna patterns: no
pattern oversampling factor: 30

Filename: Sep13_00#7 (Scenario 2)

Platform: SBR
Orbit: altitude (km) 792, inclination (deg) 98.6
Initial sub satellite point: longitude (deg) -90, latitude (deg) 47
Initial SBR direction: NORTH
peak power (watts): 5120
carrier frequency (GHz): 5.4
expanded pulse width (usec): 42
pulse bandwidth (MHz): 100
burst length (sec): 0.75
noise temperature (K): 1893
prf (Hz): 1988.3
A/D sampling rate (MHz): 112.6
waveform modulation: LFM
model receiver: yes
IF bandwidth (MHz): 112
IF filter type: Butterworth
IF filter order: 8
IF centre frequency (MHz): 1500
channel to channel mismatch (dB): -50
A/D quantization level (dB): -100
number of A/D bits: 8
number of Mismatch Ripples: 4
PRI compensation: no
ZRT compensation: no
radar system loss (dB): 0
spotlighting: no
fill pulse duration (ms): 0
model phase noise: no

thermal noise seed: 123456789
antenna seed: 232323232
clutter seed: 777777777
target seed: 567567567
jammer seed: 372372372
motion seed: 952952952
channel response seed: 101001000
available memory (MB): 800
brute-force pulse summation: no
pulse oversampling factor: 11
brute-force antenna patterns: no
pattern oversampling factor: 30

array type: phased_array
number of receive apertures: 2
grid spacing along x (m): 0.046
grid spacing along y (m): 0.046
random sidelobe level (dB): -50
physical shape: rectangular

TRANSMIT APERTURE:
x-width (m): 15
y-width (m): 0.75
x position (m): 0
y position (m): 0
x taper: uniform
y taper: uniform

RECEIVE APERTURE 1:
x-width (m): 7.5
y-width (m): 0.75
x position (m): -3.75
y position (m): 0
x taper: uniform
y taper: taylor
y sidelobe level (dB): -40

RECEIVE APERTURE 2:
x-width (m): 7.5
y-width (m): 0.75
x position (m): 3.75
y position (m): 0
x taper: uniform
y taper: taylor
y sidelobe level (dB): -40

SWATH longitude: -81.8249
swath latitude: 48.1904
swath range width (m): 1500

MECH BORESIGHT longitude: -81.8249
mech boresight latitude: 48.1904
mech boresight frd azimuth: 87.481
mech boresight elevation: 37.2849

ELEC BORESIGHT longitude: -81.8249
elec boresight latitude: 48.1904
elec boresight frd azimuth: 87.481
elec boresight elevation: 37.2849

TARGET number: 20
type: Wheeled
longitude (deg): -81.8207
latitude (deg): 48.2218
backscatter statistics: fixed
mean target RCS (m^2): 20
speed (km/h): 15
heading East of North (deg): 90
spectral width (m/s): 0

TARGET number: 19
type: Wheeled
longitude (deg): -81.8215
latitude (deg): 48.2217
backscatter statistics: fixed
mean target RCS (m^2): 20
speed (km/h): 18
heading East of North (deg): 90
spectral width (m/s): 0

TARGET number: 18
type: Wheeled
longitude (deg): -81.8222
latitude (deg): 48.2215
backscatter statistics: fixed
mean target RCS (m^2): 20
speed (km/h): 21
heading East of North (deg): 90
spectral width (m/s): 0

TARGET number: 17
type: Wheeled
longitude (deg): -81.8229
latitude (deg): 48.2214
backscatter statistics: fixed
mean target RCS (m^2): 20
speed (km/h): 24
heading East of North (deg): 90
spectral width (m/s): 0

TARGET number: 16
type: Wheeled
longitude (deg): -81.8235
latitude (deg): 48.2126
backscatter statistics: fixed
mean target RCS (m^2): 30
speed (km/h): 15
heading East of North (deg): -90
spectral width (m/s): 0

TARGET number: 15
type: Wheeled
longitude (deg): -81.8243
latitude (deg): 48.2125
backscatter statistics: fixed
mean target RCS (m^2): 30
speed (km/h): 18
heading East of North (deg): -90
spectral width (m/s): 0

TARGET number: 14
type: Wheeled
longitude (deg): -81.8251
latitude (deg): 48.2125
backscatter statistics: fixed
mean target RCS (m^2): 30
speed (km/h): 21
heading East of North (deg): -90
spectral width (m/s): 0

TARGET number: 13
type: Wheeled
longitude (deg): -81.8258
latitude (deg): 48.2123
backscatter statistics: fixed
mean target RCS (m^2): 30
speed (km/h): 24
heading East of North (deg): -90
spectral width (m/s): 0

TARGET number: 12
type: Wheeled
longitude (deg): -81.8306

latitude (deg): 48.2201
backscatter statistics: fixed
mean target RCS (m^2): 35
speed (km/h): 15
heading East of North (deg): 90
spectral width (m/s): 0

TARGET number: 11
type: Wheeled
longitude (deg): -81.8313
latitude (deg): 48.22
backscatter statistics: fixed
mean target RCS (m^2): 35
speed (km/h): 18
heading East of North (deg): 90
spectral width (m/s): 0

TARGET number: 10
type: Wheeled
longitude (deg): -81.832
latitude (deg): 48.2199
backscatter statistics: fixed
mean target RCS (m^2): 35
speed (km/h): 21
heading East of North (deg): 90
spectral width (m/s): 0

TARGET number: 9
type: Wheeled
longitude (deg): -81.8328
latitude (deg): 48.2197
backscatter statistics: fixed
mean target RCS (m^2): 35
speed (km/h): 24
heading East of North (deg): 90
spectral width (m/s): 0

TARGET number: 8
type: Wheeled
longitude (deg): -81.8345
latitude (deg): 48.2112
backscatter statistics: fixed
mean target RCS (m^2): 40
speed (km/h): 15
heading East of North (deg): -90
spectral width (m/s): 0

TARGET number: 7
type: Wheeled
longitude (deg): -81.8352
latitude (deg): 48.2111
backscatter statistics: fixed
mean target RCS (m^2): 40
speed (km/h): 18
heading East of North (deg): -90
spectral width (m/s): 0

TARGET number: 6
type: Wheeled
longitude (deg): -81.836
latitude (deg): 48.2112
backscatter statistics: fixed
mean target RCS (m^2): 40
speed (km/h): 21
heading East of North (deg): -90
spectral width (m/s): 0

TARGET number: 5
type: Wheeled
longitude (deg): -81.8368
latitude (deg): 48.211
backscatter statistics: fixed
mean target RCS (m^2): 40
speed (km/h): 24
heading East of North (deg): -90
spectral width (m/s): 0

TARGET number: 4
type: Wheeled
longitude (deg): -81.8415
latitude (deg): 48.2187
backscatter statistics: fixed
mean target RCS (m^2): 45
speed (km/h): 15
heading East of North (deg): 90
spectral width (m/s): 0

TARGET number: 3
type: Wheeled
longitude (deg): -81.8422
latitude (deg): 48.2185
backscatter statistics: fixed
mean target RCS (m^2): 45
speed (km/h): 18
heading East of North (deg): 90
spectral width (m/s): 0

TARGET number: 2
type: Wheeled
longitude (deg): -81.8429
latitude (deg): 48.2186
backscatter statistics: fixed
mean target RCS (m^2): 45
speed (km/h): 21
heading East of North (deg): 90
spectral width (m/s): 0

TARGET number: 1
type: Wheeled
longitude (deg): -81.8437
latitude (deg): 48.2184
backscatter statistics: fixed
mean target RCS (m^2): 45
speed (km/h): 24
heading East of North (deg): 90
spectral width (m/s): 0

PATCH number: 1
type: land
centre longitude (deg): -81.8324
centre latitude (deg): 48.2178
long-size (km): 2.5
lat-size (km): 5
along-range scatterer spacing (m): 2
cross-range scatterer spacing (m): 4
backscatter statistics: rayleigh
mean clutter cross-section (m^2/m^2): 0.1
spectral width (m/s): 0.1

Filename: Sep13_00#8 (Scenario 2)

thermal noise seed: 987654321
antenna seed: 323232323
clutter seed: 666666666
target seed: 765765765
jammer seed: 273273273
motion seed: 259259259
channel response seed: 10101011
available memory (MB): 800
brute-force pulse summation: no
pulse oversampling factor: 11
brute-force antenna patterns: no
pattern oversampling factor: 30

Appendix C: Signal Generation Parameters (Section 2.3)

Filename: Sep01_00#7b (Scenario 3)

Platform: SBR
Orbit: altitude (km) 792, inclination (deg) 98.6
Initial sub satellite point: longitude (deg) -90, latitude (deg) 47
Initial SBR direction: NORTH
peak power (watts): 5120
carrier frequency (GHz): 5.4
expanded pulse width (usec): 42
pulse bandwidth (MHz): 100
burst length (sec): 0.75
noise temperature (K): 1893
prf (Hz): 1988.3
A/D sampling rate (MHz): 112.6
waveform modulation: LFM
model receiver: yes
IF bandwidth (MHz): 112
IF filter type: Butterworth
IF filter order: 8
IF centre frequency (MHz): 1500
channel to channel mismatch (dB): -50
A/D quantization level (dB): -100
number of A/D bits: 8
number of Mismatch Ripples: 4
PRI compensation: no
ZRT compensation: no
radar system loss (dB): 0
spotlighting: no
fill pulse duration (ms): 0
model phase noise: no

thermal noise seed: 123456789
antenna seed: 232323232
clutter seed: 777777777
target seed: 567567567
jammer seed: 372372372
motion seed: 952952952
channel response seed: 101001000
available memory (MB): 800
brute-force pulse summation: no
pulse oversampling factor: 11
brute-force antenna patterns: no
pattern oversampling factor: 30

array type: phased_array
number of receive apertures: 2
grid spacing along x (m): 0.046
grid spacing along y (m): 0.046
random sidelobe level (dB): -50
physical shape: rectangular

TRANSMIT APERTURE:
x-width (m): 15
y-width (m): 0.75
x position (m): 0
y position (m): 0
x taper: uniform
y taper: uniform

RECEIVE APERTURE 1:
x-width (m): 7.5
y-width (m): 0.75
x position (m): -3.75
y position (m): 0
x taper: uniform
y taper: taylor
y sidelobe level (dB): -40

RECEIVE APERTURE 2:
x-width (m): 7.5
y-width (m): 0.75
x position (m): 3.75
y position (m): 0
x taper: uniform
y taper: taylor
y sidelobe level (dB): -40

SWATH longitude: -81.8249
swath latitude: 48.1904
swath range width (m): 1500

MECH BORESIGHT longitude: -81.8249
mech boresight latitude: 48.1904
mech boresight frd azimuth: 87.481
mech boresight elevation: 37.2849

ELEC BORESIGHT longitude: -81.8249
elec boresight latitude: 48.1904
elec boresight frd azimuth: 87.481
elec boresight elevation: 37.2849

TARGET number: 1
type: Wheeled
longitude (deg): -81.8466
latitude (deg): 48.2275

backscatter statistics: fixed
mean target RCS (m^2): 45
speed (km/h): 130
heading East of North (deg): 90
spectral width (m/s): 0

TARGET number: 2
type: Wheeled
longitude (deg): -81.8458
latitude (deg): 48.2276
backscatter statistics: fixed
mean target RCS (m^2): 45
speed (km/h): 120
heading East of North (deg): 90
spectral width (m/s): 0

TARGET number: 3
type: Wheeled
longitude (deg): -81.8449
latitude (deg): 48.2275
backscatter statistics: fixed
mean target RCS (m^2): 45
speed (km/h): 110
heading East of North (deg): 90
spectral width (m/s): 0

TARGET number: 4
type: Wheeled
longitude (deg): -81.8439
latitude (deg): 48.2274
backscatter statistics: fixed
mean target RCS (m^2): 45
speed (km/h): 100
heading East of North (deg): 90
spectral width (m/s): 0

TARGET number: 5
type: Wheeled
longitude (deg): -81.8349
latitude (deg): 48.2033
backscatter statistics: fixed
mean target RCS (m^2): 40
speed (km/h): 130
heading East of North (deg): -90
spectral width (m/s): 0

TARGET number: 6
type: Wheeled
longitude (deg): -81.8339
latitude (deg): 48.2039
backscatter statistics: fixed
mean target RCS (m^2): 40
speed (km/h): 120
heading East of North (deg): -90
spectral width (m/s): 0

TARGET number: 7
type: Wheeled
longitude (deg): -81.8328
latitude (deg): 48.2047
backscatter statistics: fixed
mean target RCS (m^2): 40
speed (km/h): 110
heading East of North (deg): -90
spectral width (m/s): 0

TARGET number: 8
type: Wheeled
longitude (deg): -81.8318
latitude (deg): 48.2054
backscatter statistics: fixed
mean target RCS (m^2): 40
speed (km/h): 100
heading East of North (deg): -90
spectral width (m/s): 0

TARGET number: 9
type: Wheeled
longitude (deg): -81.8349
latitude (deg): 48.2285
backscatter statistics: fixed
mean target RCS (m^2): 35
speed (km/h): 130
heading East of North (deg): 90
spectral width (m/s): 0

TARGET number: 10
type: Wheeled
longitude (deg): -81.8338
latitude (deg): 48.2284
backscatter statistics: fixed
mean target RCS (m^2): 35
speed (km/h): 120
heading East of North (deg): 90
spectral width (m/s): 0

TARGET number: 11
type: Wheeled
longitude (deg): -81.8328
latitude (deg): 48.2283
backscatter statistics: fixed
mean target RCS (m^2): 35
speed (km/h): 110
heading East of North (deg): 90
spectral width (m/s): 0

TARGET number: 12
type: Wheeled
longitude (deg): -81.8318
latitude (deg): 48.2283
backscatter statistics: fixed
mean target RCS (m^2): 35
speed (km/h): 100
heading East of North (deg): 90
spectral width (m/s): 0

TARGET number: 13
type: Wheeled
longitude (deg): -81.8243
latitude (deg): 48.204
backscatter statistics: fixed
mean target RCS (m^2): 30
speed (km/h): 130
heading East of North (deg): -90
spectral width (m/s): 0

TARGET number: 14
type: Wheeled
longitude (deg): -81.8234
latitude (deg): 48.2047
backscatter statistics: fixed
mean target RCS (m^2): 30
speed (km/h): 120
heading East of North (deg): -90
spectral width (m/s): 0

TARGET number: 15
type: Wheeled
longitude (deg): -81.8223
latitude (deg): 48.2053
backscatter statistics: fixed
mean target RCS (m^2): 30
speed (km/h): 110
heading East of North (deg): -90
spectral width (m/s): 0

TARGET number: 16
type: Wheeled
longitude (deg): -81.8213
latitude (deg): 48.206
backscatter statistics: fixed
mean target RCS (m^2): 30
speed (km/h): 100
heading East of North (deg): -90
spectral width (m/s): 0

TARGET number: 17
type: Wheeled
longitude (deg): -81.824
latitude (deg): 48.2296
backscatter statistics: fixed
mean target RCS (m^2): 20
speed (km/h): 130
heading East of North (deg): 90
spectral width (m/s): 0

TARGET number: 18
type: Wheeled
longitude (deg): -81.8231
latitude (deg): 48.2294
backscatter statistics: fixed
mean target RCS (m^2): 20
speed (km/h): 120
heading East of North (deg): 90
spectral width (m/s): 0

TARGET number: 19
type: Wheeled
longitude (deg): -81.8221
latitude (deg): 48.2291
backscatter statistics: fixed
mean target RCS (m^2): 20
speed (km/h): 110
heading East of North (deg): 90
spectral width (m/s): 0

TARGET number: 20
type: Wheeled
longitude (deg): -81.821
latitude (deg): 48.2289
backscatter statistics: fixed
mean target RCS (m^2): 20
speed (km/h): 100
heading East of North (deg): 90
spectral width (m/s): 0

PATCH number: 1
type: land
centre longitude (deg): -81.8324
centre latitude (deg): 48.2178
long-size (km): 2.5
lat-size (km): 5
along-range scatterer spacing (m): 2
cross-range scatterer spacing (m): 4
backscatter statistics: rayleigh
mean clutter cross-section (m^2/m^2): 0.1
spectral width (m/s): 0.1

SIGNAL PROCESSING PARAMETERS
Baseline: SAR
rx channel numbers: 1:2

pulse compression: yes
pulse doppler window: Hamming
pulse compression window: Hamming

SAR Pulses Used: 1:1490
SAR Replica Length: 700
BAQ bits: off

List of Acronyms

ATI	Along-Track Interferometry
CFAR	Constant False Alarm Rate
DND	Department of National Defence
DPCA	Displaced Phase Center Antenna
DREO	Defence Research Establishment Ottawa
GMTI	Ground Moving Target Indication
I-Q	In-Phase & Quadrature
MODEX	Moving Object Detection Experiment
P_{FA}	Probability of False Alarm
PRF	Pulse Repetition Frequency
PRI	Pulse Repetition Interval
R2	RADARSAT2
RCS	Radar Cross Section
SAR	Synthetic Aperture Radar
SBR	Space-Based Radar
SCR	Signal-to-Clutter Ratio
STAP	Space-Time Adaptive Processing

UNCLASSIFIED
SECURITY CLASSIFICATION OF FORM
(highest classification of Title, Abstract, Keywords)

DOCUMENT CONTROL DATA

(Security classification of title, body of abstract and indexing annotation must be entered when the overall document is classified)

1. ORIGINATOR (the name and address of the organization preparing the document. Organizations for whom the document was prepared, e.g. Establishment sponsoring a contractor's report, or tasking agency, are entered in section 8.)

Defence Research Establishment Ottawa
3701 Carling Avenue
Ottawa, Ontario, Canada K1A 0Z4

2. SECURITY CLASSIFICATION (overall security classification of the document, including special warning terms if applicable)

UNCLASSIFIED

3. TITLE (the complete document title as indicated on the title page. Its classification should be indicated by the appropriate abbreviation (S,C or U) in parentheses after the title.)

Performance of RADARSAT2 SAR-GMTI Processors at High SAR Resolutions (U)

4. AUTHORS (Last name, first name, middle initial)

Chiu, Shen

5. DATE OF PUBLICATION (month and year of publication of document)	6a. NO. OF PAGES (total containing information. Include Annexes, Appendices, etc.)	6b. NO. OF REFS (total cited in document)
December 2000	44	7

7. DESCRIPTIVE NOTES (the category of the document, e.g. technical report, technical note or memorandum. If appropriate, enter the type of report, e.g. interim, progress, summary, annual or final. Give the inclusive dates when a specific reporting period is covered.)

DREO Technical Report

8. SPONSORING ACTIVITY (the name of the department project office or laboratory sponsoring the research and development. Include the address.)

Space Systems and Technology Section, Defence Research Establishment Ottawa
3701 Carling Avenue
Ottawa, Ontario, Canada K1A 0Z4

9a. PROJECT OR GRANT NO. (if appropriate, the applicable research and development project or grant number under which the document was written. Please specify whether project or grant)	9b. CONTRACT NO. (if appropriate, the applicable number under which the document was written)
5EG11	

10a. ORIGINATOR'S DOCUMENT NUMBER (the official document number by which the document is identified by the originating activity. This number must be unique to this document.)	10b. OTHER DOCUMENT NOS. (Any other numbers which may be assigned this document either by the originator or by the sponsor)
DREO TR 2000- 093	

11. DOCUMENT AVAILABILITY (any limitations on further dissemination of the document, other than those imposed by security classification)

(x) Unlimited distribution
( ) Distribution limited to defence departments and defence contractors; further distribution only as approved
( ) Distribution limited to defence departments and Canadian defence contractors; further distribution only as approved
( ) Distribution limited to government departments and agencies; further distribution only as approved
( ) Distribution limited to defence departments; further distribution only as approved
( ) Other (please specify):

12. DOCUMENT ANNOUNCEMENT (any limitation to the bibliographic announcement of this document. This will normally correspond to the Document Availability (11). However, where further distribution (beyond the audience specified in 11) is possible, a wider announcement audience may be selected.)

13. ABSTRACT (a brief and factual summary of the document. It may also appear elsewhere in the body of the document itself. It is highly desirable that the abstract of classified documents be unclassified. Each paragraph of the abstract shall begin with an indication of the security classification of the information in the paragraph (unless the document itself is unclassified) represented as (S), (C), or (U). It is not necessary to include here abstracts in both official languages unless the text is bilingual).

Canada's RADARSAT2 commercial SAR satellite, scheduled to be launched in Spring 2003, will have an experimental operating mode that will permit ground moving target indication (GMTI) measurements to be made with received data. In this mode of operation, the radar antenna is partitioned into two sub-apertures that sequentially observe the scene of interest from the same points in space. Two GMTI processing approaches are currently being explored. One utilizes the classical SAR/DPCA clutter cancellation technique to provide sub-clutter visibility for dim slowly moving objects. The other is based on the along-track (temporal) SAR interferometer (SAR/ATI) technique, where amplitude and phase information of the targets are exploited to extract them from the background clutter. In this paper the performance of each processor is examined for RADARSAT2's ultrafine beam mode. The study focuses on the influence of SAR resolution cell size on the GMTI processor performance. Results indicate that at high SAR resolutions the SAR/ATI is a better technique compared to the SAR/DPCA in its ability to detect slow-moving targets.

14. KEYWORDS, DESCRIPTORS or IDENTIFIERS (technically meaningful terms or short phrases that characterize a document and could be helpful in cataloguing the document. They should be selected so that no security classification is required. Identifiers such as equipment model designation, trade name, military project code name, geographic location may also be included. If possible keywords should be selected from a published thesaurus. e.g. Thesaurus of Engineering and Scientific Terms (TEST) and that thesaurus-identified. If it is not possible to select indexing terms which are Unclassified, the classification of each should be indicated as with the title.)

SAR, GMTI, ATI, DPCA
Synthetic aperture radar
Ground moving target indication
Along-track interferometry
Displaced phase center antenna